



UNIVERSITÀ DEGLI STUDI DI GENOVA

DIPARTIMENTO DI SCIENZE DELLA TERRA, DELL'AMBIENTE E DELLA VITA

Corso di Laurea Magistrale in Hydrography and Oceanography

**Refinement and Automation
of Satellite Derived Bathymetry and
Development of a new Software Tool**

Dafrosa John Kataraihya

Relatori:

Prof. Matteo Guideri

Correlatori:

Prof.ssa Paola Picco

Anno Accademico 2020/2021



UNIVERSITÀ DEGLI STUDI DI GENOVA

DIPARTIMENTO DI SCIENZE DELLA TERRA, DELL'AMBIENTE E DELLA VITA

Corso di Laurea Magistrale in Hydrography and Oceanography

**Refinement and Automation
of Satellite Derived Bathymetry and
Development of a new Software Tool**

Dafrosa John Kataraihya

Relatori:

Prof. Matteo Guideri

Correlatori:

Prof.ssa Paola Picco

Anno Accademico 2020/2021

ABSTRACT

Mapping the seabed is an essential part of understanding the earth's waterbodies. Different techniques have been evolving over the years since the 1970s. Satellite Derived Bathymetry (SDB) a newly evolving technology has proved useful in determining depth at shallow and gently sloping areas. The technology has grown in the last ten years due to the availability of multi-constellation, multi-temporal, and multi-resolution remote sensing data as Open Data. Effective SDB algorithms have been proposed by many authors, but further research on their performance is needed as well as an efficient way on how to process this data is needed to simplify the workflow. Hence the main objective of this thesis is to further refine the Stumpf and Lyzenga algorithms, used for depth derivation and develop a tool which would facilitate quick and reliable workflow in a GIS environment The Stumpf algorithm was refined by further evaluating logarithmic and 2nd order polynomial regressions, while the Lyzenga algorithm investigated the performance of different band pairs.

The tool developed was intended for use in QGIS. The tool's name is 'SDB Automate'. It was developed using Python programming language, GDAL libraries and QT designer for Graphic User Interface (GUI). The tool reduced the processing time from 6 hours to approximately 8 minutes.

Validation was done around La Spezia and Livorno for 3 consecutive years 2017, 2018 and 2019. Both linear and log showed similar results in the Stumpf workflow with an error range of 0.5m to 1.2m while Lyzenga (blue-green band) showed best results, but for areas with suspension or river flow the green-red band showed better results with the overall error range being 0.65m to 1.6m.

Keywords

Satellite Derived Bathymetry, QGIS, Stumpf, Lyzenga, multispectral images

Table of Contents

ABSTRACT.....	3
ACKNOWLEDGMENT.....	6
LIST OF FIGURES	7
LIST OF TABLES.....	8
1. CHAPTER ONE.....	9
1.1. INTRODUCTION.....	9
1.2. RESEARCH OBJECTIVES AND THESIS STRUCTURE.....	10
2. CHAPTER TWO: BACKGROUND/ LITERATURE REVIEW	12
2.1. HISTORY OF HYDROGRAPHIC SURVEYS	12
2.2. INTRODUCTION TO REMOTE SENSING	13
2.2.1. Types of Satellites and their orbits.....	13
2.2.2. Remote Sensing Techniques	14
2.2.3. Solar Irradiance.....	15
2.2.4. Electromagnetic Radiation.....	16
2.3. SATELLITE DERIVED BATHYMETRY	17
2.3.1. Factors affecting light attenuation in satellite images.....	18
2.4. PHYSICS AND EMPIRICAL APPROACH.....	20
2.4.1. Empirical based approach	20
2.4.2. Physics based approach.....	22
3. CHAPTER THREE: METHODOLOGY	23
3.1. DESIGNING THE ‘SDB AUTOMATE’ PLUGIN.....	23
3.1.1. System Environment.....	23
3.1.2. Plugin Presentation	23
3.2. IMPLEMENTATION OF SDB ALGORITHM IN ‘SDB AUTOMATE PLUGIN’.....	25
3.2.1. Delineating the water area	25
3.2.2. Stumpf algorithm as implemented in the plugin.....	26
3.2.3. Lyzenga algorithm as implemented in the plugin.....	29
3.3. RESEARCH AREA AND DATA	31
3.3.1. Research Area	31
3.3.2. Data.....	32
3.4. VALIDATION OF THE PLUGIN	35
3.4.1. Pre-Processing.....	35
3.4.2. Stumpf Validation.....	36
3.4.3. Lyzenga validation.....	40

4. CHAPTER FOUR: DISCUSSION AND RESULTS ANALYSIS	45
4.1. PLUGIN WORKING ENVIRONMENTS	45
4.2. SATELLITE DERIVED BATHYMETRY	45
4.2.1. Stumpf workflow Results	45
4.2.2. Lyzenga Workflow Results.....	46
4.2.3. Workaround of the Physics Approach to SDB	46
5. CHAPTER FIVE: CONCLUSION AND RECOMMENDATION	47
5.1. Conclusion.....	47
5.2. Recommendations	47
REFERENCES	48

ACKNOWLEDGMENT

I would love to thank God for his love and mercies towards me during this whole master's program, it wouldn't have been possible without him.

I would also like to thank my supervisors Dr. Matteo Guideri and Prof. Paola Picco for their continued guidance, willingness to teach me and setting aside their precious time to read and correct my thesis work. This would never have been a success without them. Thank you so much.

Furthermore, I thank my family who have been my constant support system, though they have been miles away from me, but they always managed to reach out whenever I needed them. I am forever indebted.

My thanks and appreciation also goes out to my friend Cris Thomas, who has constantly been there for me whenever I needed assistance. He has been kind and compassionate and always there to listen to me even when I made absolutely no sense.

Additionally, I extend my gratitude towards my colleagues, they have been the family I never had once I stepped foot in Italy. We started as strangers but later became family. They made my life a lot easier in Italy. I'll forever be indebted.

LIST OF FIGURES

Figure 1: Evolution of hydrographic survey	12
Figure 2: Satellite's Orbiting systems	14
Figure 3: Active and passive sensors system examples	15
Figure 4: Solar Irradiance at the top of atmosphere and at sea level	16
Figure 5: Electromagnetic spectrum highlighting the visible band.Source: https://chem.libretexts.org/	17
Figure 6: Behaviour of blue, green and red bands in both coastal and oceanic waters and the percentage of transmittance in both conditions.....	18
Figure 7: Factors affecting the signal received by the satellites. Source: (Westley, 2021).....	20
Figure 8: Creation of the plugin's user interface in Qt designer.....	24
Figure 9: Diagram elaborating the internal structure of the plugin and how each file is linked until its representation in QGIS.	24
Figure 10: Diagrammatical representation of the Stumpf algorithm workflow as implemented in the plugin	26
Figure 11: Narrates on the vertical referencing (a) display of the regression points where the user selects the points in relative to the distribution (b) the selection process (c) the display of all the regression lines created i.e., linear, log and polynomial.	28
Figure 12: Plugin user interface presentation while running the Stumpf algorithm as is displayed for use in QGIS.....	28
Figure 13: Lyzenga algorithm workflow as implemented in the plugin.....	30
Figure 14: Plugin user interface presentation while running the Lyzenga algorithm as is displayed for use in QGIS.....	31
Figure 15: Map depicting the study area.....	32
Figure 16: Electronic Navigation Chart (ENC) tiles in red, used for validating the tool.....	33
Figure 17: (a), (b), (c) depicting the image selection and downloading process	34
Figure 18: Distribution of control points based on IT400115 &IT400120 ENCs, and the red line indicating the slicing area of the image into image A (La Spezia) and image B (Livorno).....	35
Figure 19: Final output display while running the Stumpf algorithm.....	36
Figure 20: (a)-2017, (b)-2018, (c)-2019, calculating the gain and offset using the control points and the ratio between blue and green band (raster value).....	37
Figure 21: Sample of Stumpf SDB variants derived from Sentinel-2 imagery for La Spezia (L.H.S) and Livorno (R.H.S) for 2017, colour ramp indicates the depth variation.	40
Figure 22: Final output display using Lyzenga algorithm	40
Figure 23: Sample of Lyzenga SDB variants derived from Sentinel-2 imagery for La Spezia (L.H.S) and Livorno (R.H.S) for 2017 colour ramp indicates the depth variation.	42

LIST OF TABLES

Table 1: Satellite Images used in the plugin	34
Table 2: Summary of SDB algorithms used and the band pairs	35
Table 3: Values obtained in vertical Referencing	38
Table 4: Multiple Linear regressions coefficients for each band pair of 2017, 2018 and 2019 images at La Spezia and Livorno.	42
Table 5: SDB algorithm performance: Root Mean Square Error (RMSE: average difference with the ground truth points), R2 values (indicating how well the SDB algorithms fit their trendlines and error range (full range difference with the ground control points) at La Spezia.	43
Table 6: SDB algorithm performance: Root Mean Square Error (RMSE: average difference with the ground truth points), R2 values (indicating how well the SDB algorithms fit their trendlines and error range (full range difference with the ground control points) at Livorno.	43
Table 7: Plugin working environments and time used while processing SDB algorithms	45

1. CHAPTER ONE

1.1.INTRODUCTION

Mapping the waterbodies has become increasingly important as many activities now depend on the waterbodies i.e., from navigation, fishing, trade, tourism to entertainment. Hence adequate information about the seabed is needed for one to make informed decisions, create policies and undertake different scientific research. (Seabed 2030)

There are currently many different techniques that are used to map the seabed both using the standard hydrographic methods and remote ways. The standard hydrographic methods involve the use of multi beam echo sounder (MBES), single beam echosounder (SBES) and side scan sonar (SSS) which prove to be expensive in both time and price which results to seldom surveying of some maritime regions but provides high accuracy. Whereas the remote ways have proven to be fast and less expensive though at the expense of data accuracy. Some of the remote ways involve the use of Light Detection And Ranging (LiDAR) and satellites. In which both are limited to coastal, intertidal and shallow water areas.

The introduction of Satellite Derived Bathymetry (SDB) can compensate for the short comings of the standard hydrographic surveys. According to (Shachak Pe'eri, Christopher Parrish,Chukwuma Azuike, Lee Alexander Andrew Armstrong, 2014), this method proved to be effective for reconnaissance survey by providing depth estimation from satellite imagery and control points which can be derived from nautical charts, single beam echosounder or multibeam echosounder through establishing a linear relationship. Due to the free access to public available satellite imagery e.g. Landsat 8, Sentinel 2A which provide a global coverage within a short period of time, and access to the most difficult areas where a ship or boat equipped with an echo sounder could not reach, this method can be used to infer bathymetry and analyse the bathymetry changes at a region of interest.

According to (Richard P. Stumpf, Kristine Holderied, Mark Sinclair, 2003), the SDB approach model assumes a uniform seabed which means the values of reflectance and water attenuation are constant throughout the Region of Interest (ROI). This implies no environmental changes can affect the depth determination. Hence, a linear relationship exists between the SDB model and the calibration points.

SDB model is mostly applicable on areas with clear waters and a continuous beach especially sandy bottoms mainly tropical and subtropical regions, also (GEBCO, 2019) suggests areas with a depth ranging from 1 to 2 metres up to 12 metres. Above or below this limit SDB is

affected by waves or water mixing caused at the beach. Furthermore, when performing SDB calculations, there is no need to measure the tide since the control points used to vertically reference the SDB model, are already referenced to the respective chart datum.

Although the SDB method is simple, it has some limitations

- ❖ SDB method is used as a reconnaissance tool, to map near-shore bathymetry, characterize coastal area and to monitor seafloor changes that may have occurred since the last hydrographic survey was conducted it is not designed to replace the traditional methods but if improved could attain an acceptable accuracy.
- ❖ SDB method requires one to perform depth computations repetitively if one uses different images for processing, since the images are being updated every after a few days and with different resolution depending on the satellite sensor used to capture the images.
- ❖ SDB methods requires a lot of time if one has many images to process since each image should be processed separately at a time.

The above limitations are the primary focus of this thesis.

1.2.RESEARCH OBJECTIVES AND THESIS STRUCTURE

SDB technique has shown tremendous growth as a method of deriving bathymetry in recent years. However, most of the approach has been based on the Stumpf procedure neglecting the Lyzenga procedure. Hence the potential of SDB technique is not fully explored.

Also, the traditional hydrography cannot be performed on very shallow areas since shallow areas impose a danger to navigation meaning the hydrographic instrumentation may be affected by the underlying features, hence causing a shipwreck.

Therefore, the main objective of this thesis is to further research on remote ways used on SDB both the Stumpf procedure (Stumpf et al 2003) and the Lyzenga procedure (Lyzenga 1978, 1985) by creating a fast but efficient tool for processing the SDB. The tool will enable availability of bathymetric information in areas that have not been surveyed by the traditional hydrography or no updated/reliable chart.

The following is a brief outline of the whole thesis

Chapter 2 explains on the previous SDB related studies and how hydrographic methods have evolved over time.

Chapter 3 explains on the methodology which includes the study area, data used and how the tool was created this involves description of the programming language used and why it was used, the GUI creation, how the tool was validated, and the results obtained.

Chapter 4 discusses and analyses the results.

Chapter 5 concludes the thesis and recommends on the way forward.

2. CHAPTER TWO: BACKGROUND/ LITERATURE REVIEW

2.1. HISTORY OF HYDROGRAPHIC SURVEYS

The science of understanding, measuring and describing features that affect safety of navigation, offshore construction, oil exploration, dredging and related activities is referred as hydrographic surveying. Whereas depth determination and determination of the underwater topology is referred to as bathymetry.

Generally, both techniques date as back as the 16th Century where the first nautical chart was produced. Through using different systems, equipment and procedures, hydrographic surveys were conducted. In the early days, sounding/ depth was derived using a lead line and a sounding pole. As technology progressed, in the mid 1900's Single Beam Echo Sounder (SBES) were developed and used. Side Scan Sonar (SSS) was later used in the 1970's but was mainly deployed for object detection and not bathymetry because it could provide underwater images. Later in the 1990's Multibeam Echo Sounder (MBES) came into operation. These techniques enabled advancement in understanding the underwater world (fig 1).

Currently, the SBES, MBES and SSS are the most common used techniques, though these techniques provide high accuracy that fits the International Hydrographic Organisation (IHO) standards, they are expensive in terms of logistics and management, cost and time.

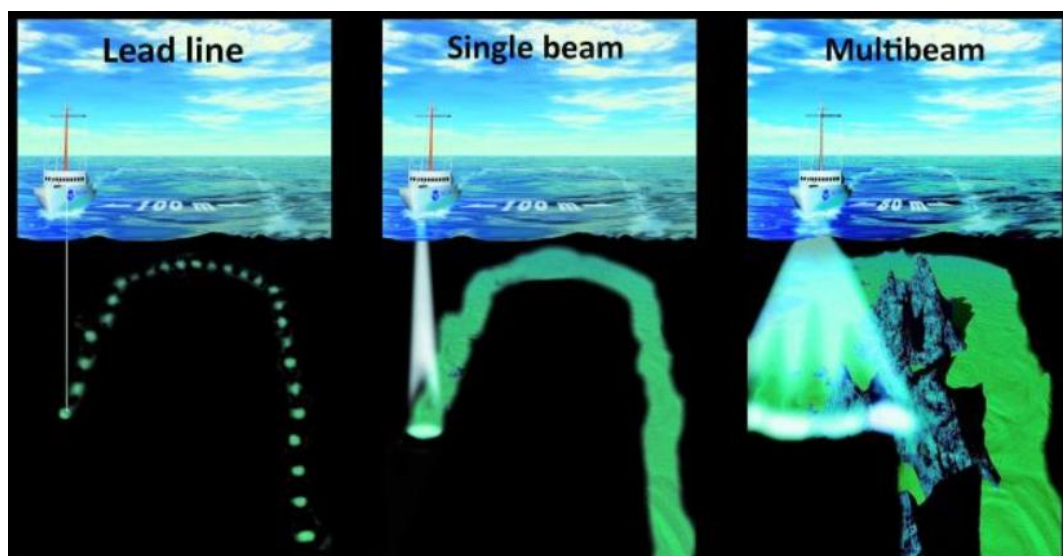


Figure 1: Evolution of hydrographic survey

Source: <https://www.hydro-international.com/>

2.2.INTRODUCTION TO REMOTE SENSING

Remote Sensing (RS) is the use of electromagnetic radiation to obtain information about different geospatial entities like the ocean, atmosphere, or land without physical contact with the intended feature under observation. RS measurements observe wide areas indirectly within a short period of time. Most observed phenomenon are inferred from emitted or reflected radiation. The RS sensors can range from multispectral satellite imager e.g., Landsat 8 uses the Operational Land Imager (OLI) and the Thermal Infrared Sensor (TIRS) while Sentinel 2 uses MSI sensors, radiometer mounted either on an aircraft, oil platform or ship.

Considering that satellite sensors are situated miles away from the phenomena under observation, it is necessary to consider the frequency and intensity distribution of the reflected radiation. The reflected radiation distribution depends on how the emitted radiation was generated and modified as it propagated through different mediums i.e., air or water, Also, properties of the reflected radiation depends on the type of sensor used. The sensor must be capable of observing and monitoring wavelengths that are applicable for the observed phenomenon.

2.2.1. Types of Satellites and their orbits

According to (Martin, 2014), there are two kinds of satellites, natural and manmade. For this thesis, only the manmade satellites will be discussed.

The satellites are of different types depending on what they are set to observe and their satellite orbiting system.

Satellite orbiting system

The satellite's orbit relative to the Earth is divided into two aspects, the satellite motion in its orbit plane relative to the centre of mass of Earth and the satellite position relative to the rotating Earth. There are three common orbits sun-synchronous, geosynchronous and low-inclination orbits as shown in fig 2.

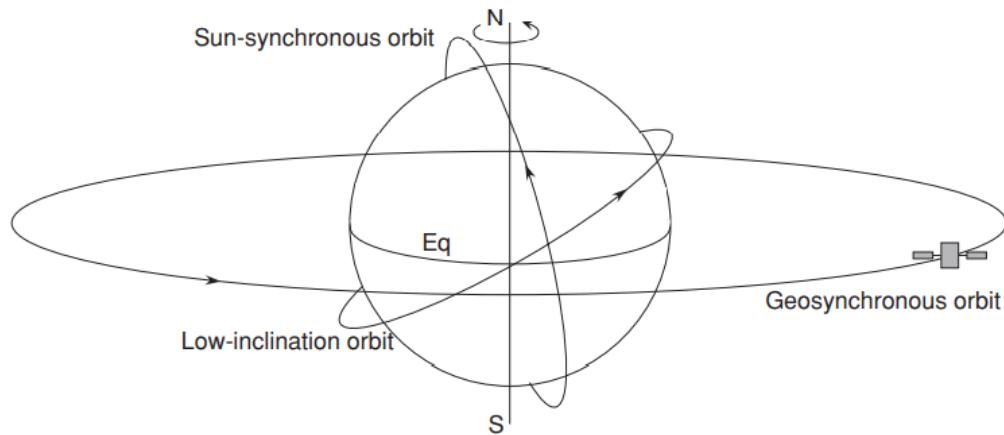


Figure 2: Satellite's Orbiting systems

- i. The geosynchronous orbit (GEO) – Is located about 35800km above the Earth's equatorial plane (equator = 0). It is fixed at one location such that it continuously observes the same surface area e.g., the telecommunication satellites. The revolution period of a geosynchronous satellite is 23.93 hours, which is the time the Earth rotates around its own axis.
- ii. The sun-synchronous orbit -- Is located about 800km from the Earth's surface and is situated at about (90 degrees) N or S of the Equator. The sun-synchronous satellites take approximately 90 minutes to orbit around the earth making around 16 orbits per day. Its name come as a result that each orbit crosses the equator at the same local time of the day. Hence these satellites are used for monitoring the ocean phenomenon such as SST, chlorophyll.
- iii. Low-inclination orbit—This includes both the low earth orbit (LEO) and the Medium Earth Orbit (MEO). The satellites in the low inclination orbit are relatively close to the earth's surface unlike the GEO satellites. These range anywhere below 1000 km in altitude, and they do not have a fixed path. Hence can orbit anywhere on the Earth's surface. Since these satellites are very close to the Earth, they are mostly used for satellite imaging or navigation purposes because they produce a high resolution.

2.2.2. Remote Sensing Techniques

- i. Active Remote Sensing

This involves the use of active sensors which produce their own light source. They send a pulse and measure the backscattered signals. The intensity of the backscattered signal may be different to the emitted signal due to absorption, scattering and reflection. The most common active sensor used in remote sensing is the radar, e.g. the Synthetic Aperture Radar (SAR). These sensors operate in the microwave and radio wavelength regions of the electromagnetic spectrum, with wavelength ranging from 1mm to 20m. The main advantage of active sensors is, it can collect data continuously (day and night) and passes through clouds and gaseous due to its low frequency and long wavelength.

ii. Passive remote sensing

These sensors mainly measure the reflected sunlight energy from an object (solar irradiance). The sun is the source of light to all observed phenomena. Example of these sensors are the multispectral sensors. These are specialized to measure a certain range of wavelength but are cloud-free restricted e.g., Sentinel 2, Landsat 8.



Figure 3: Active and passive sensors system examples

2.2.3. Solar Irradiance

Active satellite sensors are used to calculate bathymetry. Hence it is important to understand how the sun energy (solar irradiance) behaves in water. Solar irradiance is the amount of light energy emitted by the sun to the Earth per time per unit area. This light energy is dissipated in form of electromagnetic radiation power and attenuates as it approaches the Earth's surface. The sea level's solar irradiance can be calculated if the Sun is approximated as a black body at 6000K. At the top of atmosphere (TOA), the solar irradiance is 1367 W.m^{-2} while at the sea level the solar irradiance in the visible wavelength it is 522 W.m^{-2} whereby it is 38.2% of the total solar irradiance, as shown on fig 4.

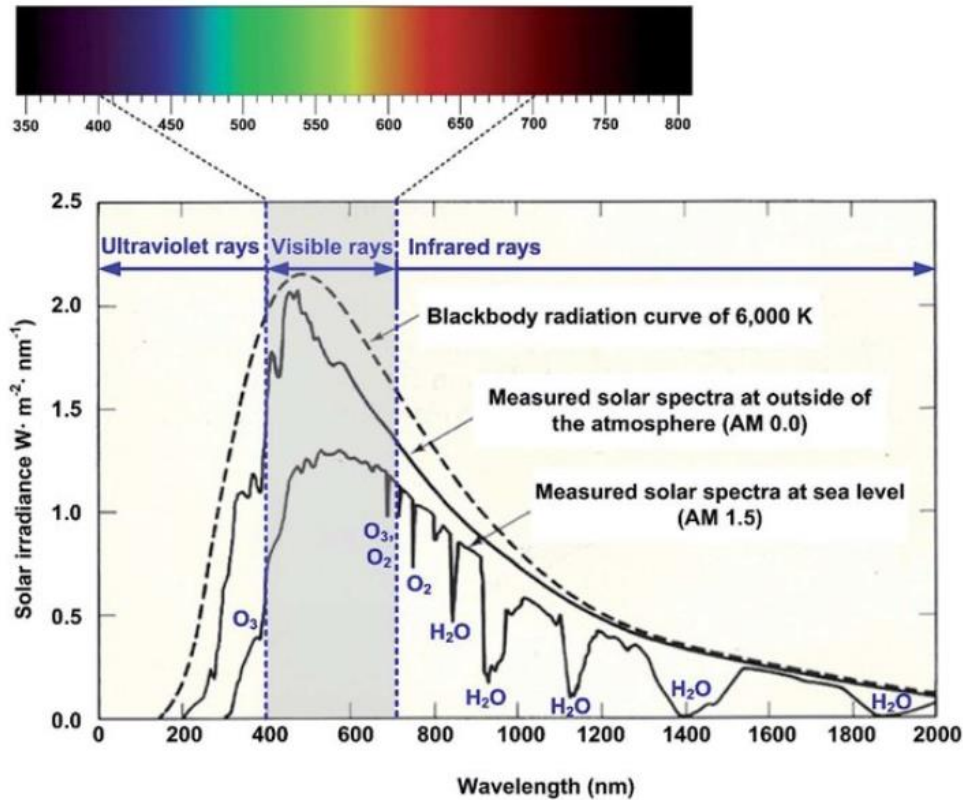


Figure 4: Solar Irradiance at the top of atmosphere and at sea level

2.2.4. Electromagnetic Radiation

The electromagnetic spectrum is the continuum of energy ranging of wavelength from kilometers to nanometers. Spectral bands are the division of the continuum into ranges, and the boundaries between them are gradational. So, the electromagnetic spectrum ranges from the shorter wavelengths (including gamma and x-rays) to the longer wavelengths (including microwaves and broadcast radio waves). Therefore, there are many electromagnetic waves useful in remote sensing. Figure 5 shows the ranges of wavelengths and frequencies for each individual portion of electromagnetic spectrum while highlighting the visible band. Most Earth observation instruments such as regular cameras, passively record Electromagnetic radiation in the visible part of the spectrum approximately 400 to 700 nanometres, NIR approximately 700 to 1100 nanometres whereas SWIR spans from approximately 1200-2400 nanometres. The discovery of electromagnetic spectrum enabled great advancement in remote sensing.

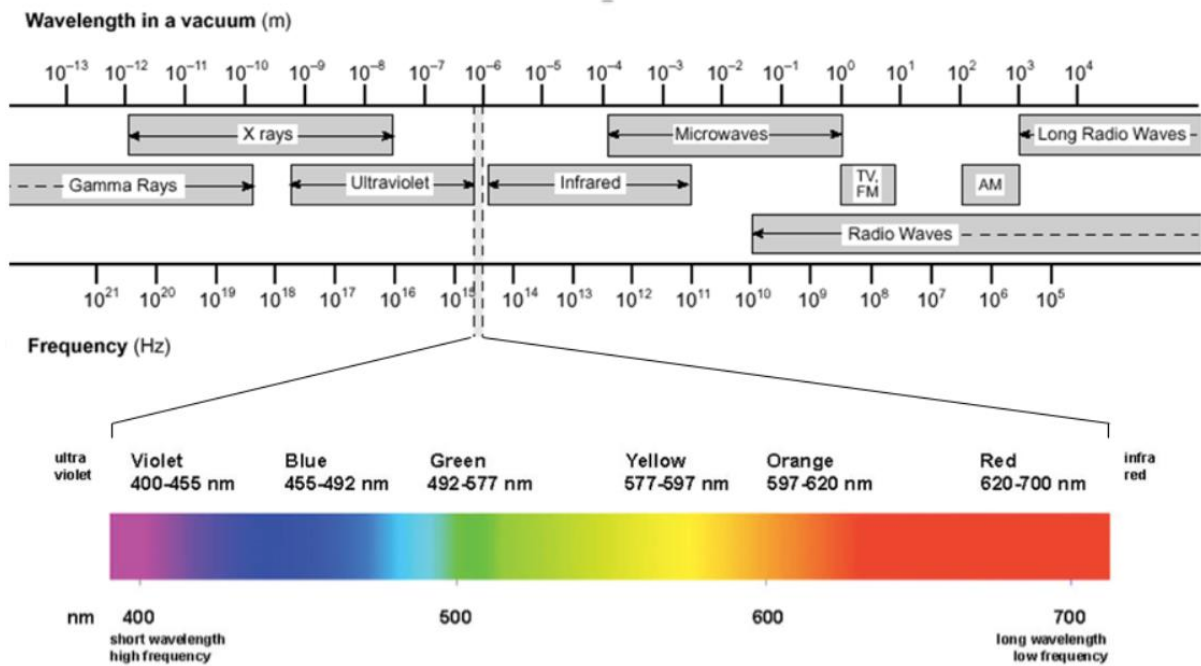


Figure 5: Electromagnetic spectrum highlighting the visible band. Source: <https://chem.libretexts.org/>

2.3.SATELLITE DERIVED BATHYMETRY

Satellite Derived Bathymetry (SDB) generally addresses bathymetry/ water depth derived from space-based techniques. Some of which are multispectral imagery e.g., Landsat and Sentinel images, Light Detection And Ranging (LiDAR) and approaches that rely on gravity measurements e.g., satellite altimetry. For this thesis, multispectral images were used to derive the bathymetry.

Bathymetry is derived from the images by considering how the electromagnetic radiation (light) penetrates the water column and gets reflected from the seafloor. But it should be known that light attenuates as the water depth increases. As satellites observe from above, the shallow water areas appear bright since light penetrates the water and is reflected from the seafloor while the deeper water areas appear dark since light is absorbed before it reaches the seafloor. Figure 6 describes how the green, blue and red band behaves in water based on different conditions and wavelength. But also the sunlight reflection on the water surface can alter the appearance of the images. It may make the water look grey, silver or white.

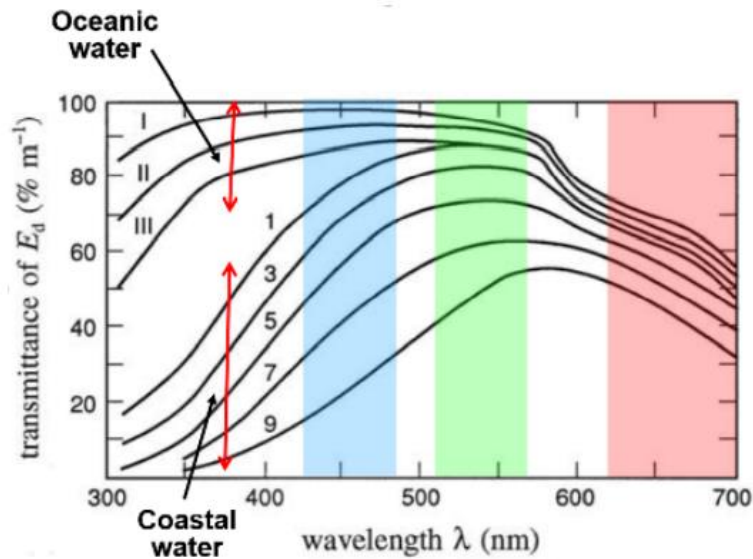


Figure 6: Behaviour of blue, green and red bands in both coastal and oceanic waters and the percentage of transmittance in both conditions.

2.3.1. Factors affecting light attenuation in satellite images

i. Sun glint

Sun glint is mostly observed in high spatial resolution remote sensing imagery data. The problem occurs when the surface of water is not flat, and the sun radiation is directly reflected to the sensor affecting the pixel brightness values. (G. Doxani, M. Papadopoulou, P. Lafazani, M. Tsakiri - Strati., 2009). Water surface state, sun position and viewing angle of the sensors are the main function parameters to estimate glint effect on the images. The removal of glint is necessary since multispectral bathymetry and bottom types mapping are highly affected. Hence removing sun glint will clean the image and leave it with water irradiance only.

How to eliminate Sun glint effect

There are different sun glint correction algorithms like (John F. Mustard, Matthew I. Staid, William J. Fripp, 2001), (John Hedley, Alastair Harborne, Peter Mumby, 2005), (D. R. Lyzenga, N. P. Malinas, F. J. Tanis, 2006) and (Tiit Kutser, Ele Vahtmäe, Jaan Praks, 2009) but according to (Miller, 2012) the Lyzenga method proved to be the best. According to his approach, sun glint is estimated by utilizing the covariance of visible band used for depth processing and the near-infrared band. Considering that water highly absorbs the NIR band, it results to pixel brightness value close to zero, in case of higher pixel values should imply atmospheric or glint effect.

Glint estimation function ignoring the atmospheric effect is dR_{VIS} :

$$dR_{VIS} = \frac{\sigma_{VIS,NIR}}{\sigma_{NIR}^2} (R_{NIR} - Mean_{NIR}) \dots\dots\dots 1$$

where VIS= visible band, NIR= infrared band, $\sigma_{VIS,NIR}$ is the covariance coefficient of visible and infrared band, σ_{NIR}^2 is the variance coefficient of infrared band, R_{NIR} is the pixel value in NIR band, $Mean_{NIR}$ is the average of a deep-water sample of pixels in NIR band.

The corrected pixel value R'_{VIS} is then calculated by subtracting the ‘glint quantity’ from the visible glinted band R_{VIS} :

$$R'_{VIS} = R_{VIS} - dR_{VIS} \dots\dots\dots 2$$

Combining equations 1 and 2 above:

$$R'_{VIS} = R_{VIS} - r(R_{NIR} - Mean_{NIR}) \dots\dots\dots 3$$

Where r is the coefficient, $r = \frac{\sigma_{VIS,NIR}}{\sigma_{NIR}^2}$

ii. Light wavelength

The long wavelengths are absorbed by water while the short wavelength e.g., blue and green penetrate the water column and gets reflected from the seafloor.

iii. Atmospheric correction

It includes the clouds and smoke, where the clouds may cast dark shadows on the images enhancing the original shape of the clouds. And they may be observed as white or grey. While smoke is smoother than clouds and is presented in brown to grey colour. There are many ways to correct for the atmospheric error, but they usually require atmospheric and sea water conditions which are difficult to obtain. Hence (Benny and Dawson 1983) proposed a simplified method which involves subtraction of dark pixels from the raster values pixels (Equation 4). But this method is useful only when the atmospheric behaviour is the same throughout the ROI.

$$R_{AC} = R_i - R_{dp} \dots\dots\dots 4$$

Where R_{AC} is the atmospherically corrected pixel value, R_i is the initial pixel value and R_{dp} is the dark pixel value.

iv. Turbidity

This considers the presence of particulate organic matter (POM), Coloured Dissolved Organic Matter (CDOM), phytoplankton and as a result alters the colour of water. Once colour changes in water so does the increase of absorption of light which leads to a decrease of a remote sensing signal penetration in water.

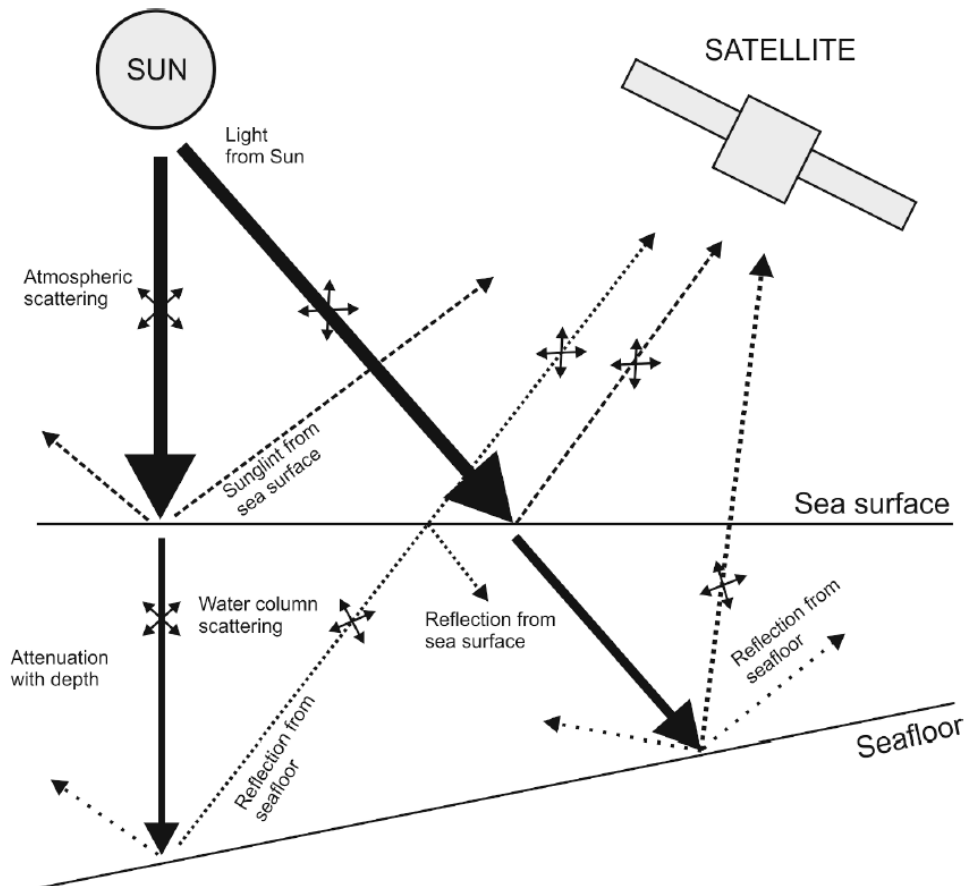


Figure 7: Factors affecting the signal received by the satellites. Source: (Westley, 2021)

2.4. PHYSICS AND EMPIRICAL METHODS

In order to obtain SDB, two methods can be used i.e., Empirical based method and Physics based method.

2.4.1. Empirical based method

Empirical based approach requires analysing a relationship between in-situ depth data and their corresponding reflectance from the spectral bands of the remotely sensed image. This approach requires depth data from either nautical chart, geophysical or oceanographic surveys involving acoustic instrumentation e.g., Single Beam Echo Sounder (SBES), Multibeam Echo Sounder (MBES) or airborne LiDAR to be used as control points as well as for calibration. After

obtaining the relationship through regression, the regression coefficients are applied to the whole satellite image in order to obtain bathymetry.

2.4.1.1. Lyzenga Model (Linear Band ratio)

Around 1960s the use of passive sensors in deriving bathymetry was discovered by (Polcyn, F.C., and Rollin, R.A., 1969). This technique was based on obtaining a linear relationship between depth and the reflectance values. A good correlation is attained when the bottom reflectance and the optical properties are uniform, if not more than one wavelength is to be used for depth calibration (Lyzenga, 1985). Equation 5 shows the proposed water reflectance model which elaborates on how a passive sensor would receive a signal from shallow waters neglecting the effect of signal scattering in water and signal's internal reflection.

$$L_i = L_{si} + k_i r_{Bi} \exp(-\kappa_i f z) \dots\dots\dots 5$$

Where L_{si} is the radiance from deep water (reflection from the water surface and atmospheric scattering), k_i is a constant which combines solar irradiance, atmosphere and water surface transmittance and radiance reduction due to water surface reflectance, r_{Bi} is bottom surface reflectance, κ_i is water attenuation coefficient, f is a geometric factor accounting for pathlength, and z is the water depth.

According to (Polcyn, F.C., and Rollin, R.A., 1969), it was assumed the ratio of bottom reflectance is the same for all given bottom types, hence generating Equation 6.

$$\frac{r_{A1}}{r_{A2}} = \frac{r_{B1}}{r_{B2}} = R_b \dots\dots\dots 6$$

Inverting equation (6) and solving the left hand side (LHS)

$$z = \frac{1}{(\kappa_1 - \kappa_2) f} \left[\ln \frac{\kappa_1}{\kappa_2} - \ln \frac{R}{R_b} \right] \dots\dots\dots 7$$

Where R is the ratio of bottom reflectance in 2 bands.

$$R = \frac{L_1 - L_{S1}}{L_2 - L_{S2}} \dots\dots\dots 8$$

If equation 6 is correct, depth is calculated from the bottom surface.. Therefore the use of multiple pair of bands is advised. Hence the linear band ratio developed by (Lyzenga, 1978).

$$Z = a_0 + a_1X_1 + a_2X_2 \dots\dots\dots 9$$

$$X = \ln(L_i - L_{si})\dots\dots\dots 10$$

Where Z is the water depth, a_0 , a_1 , a_2 are constants derived from multiple linear regression calculated from X1, X2 and control depth.

2.4.1.2. Stumpf Model (Ratio Transformation)

(Richard P. Stumpf, Kristine Holderied, Mark Sinclair, 2003) developed a way to derive bathymetry by using the ratio of two visible bands i.e., the green and blue band. The reflectance from these bands had only two tuneable constants and could be applicable at areas with low albedo. The Stumpf algorithm is:

$$Z = m_1 \left(\frac{\ln(n \cdot R_W(\lambda_i))}{\ln(n \cdot R_W(\lambda_j))} \right) - m_0 \dots\dots\dots 11$$

Where z is depth, n is a fixed constant for all areas (it ensures all values of log are positive), m_1 and m_0 are tuneable constants and offset used for calibrating the model, R_W denotes the reflectance from both green and blue band.

2.4.2. Physics based approach

Physics based approach does not need in-situ control depth points but rather focuses on understanding/analysing how light behaves in water and how it is affected by suspended particulate matter, seafloor reflectance, environmental factors e.g., wind, sun angle etc., depth and wavelength.

This approach can derive depth by using the radiative scattering models. These models define the scattering and absorption of electromagnetic radiation. It requires seafloor reflectance representing a wide variety of seafloor types and a wide range of water quality parameters. (Lee, Z., Carder, K. L., Mobley, C. D., Steward, R. G., & Patch, J. S., 1999). This data is then stored on a Look-Up Table for processing.

3. CHAPTER THREE: METHODOLOGY

3.1.DESIGNING THE ‘SDB AUTOMATE’ PLUGIN

3.1.1. System Environment

The ‘SDB Automate plugin’ used to estimate near shore bathymetry was developed for use in Quantum GIS (QGIS). QGIS is an open-source platform used for viewing, interpreting and analysing variety of geospatial data. It is widely used in academia, governmental and commercial environments. The availability of different libraries like GDAL, OSGEO and the incorporating of Python scripting library/console assists in implementing numerous customizable modules for geoprocessing.

Python, a widely used programming language which provides a powerful scripting environment in QGIS, enables users to efficiently exploit the capabilities of QGIS software for developing new plugins. The availability of different packages in Python made programming of ‘SDB Automate’ easier to manipulate. Some of the packages are *numpy*, *pandas*, *utm*, *sklearn*, *scipy*, *matplotlib* etc. Each package gives a different solution depending on the task to be implemented. Python libraries combined with QGIS libraries helped in implementing the SDB algorithms both in Stumpf and Lyzenga.

3.1.2. Plugin Presentation

This plugin used ‘QT designer’ to create an interface. QT designer is a tool used for building and designing graphical user interface (GUIs) using QT widgets. It allows one to simply design an interface as they would want it to appear. QT designer can be linked to Python hence on QGIS. The figure 8 and 9 below show the general structure/ environment of how the plugin is designed and linked.

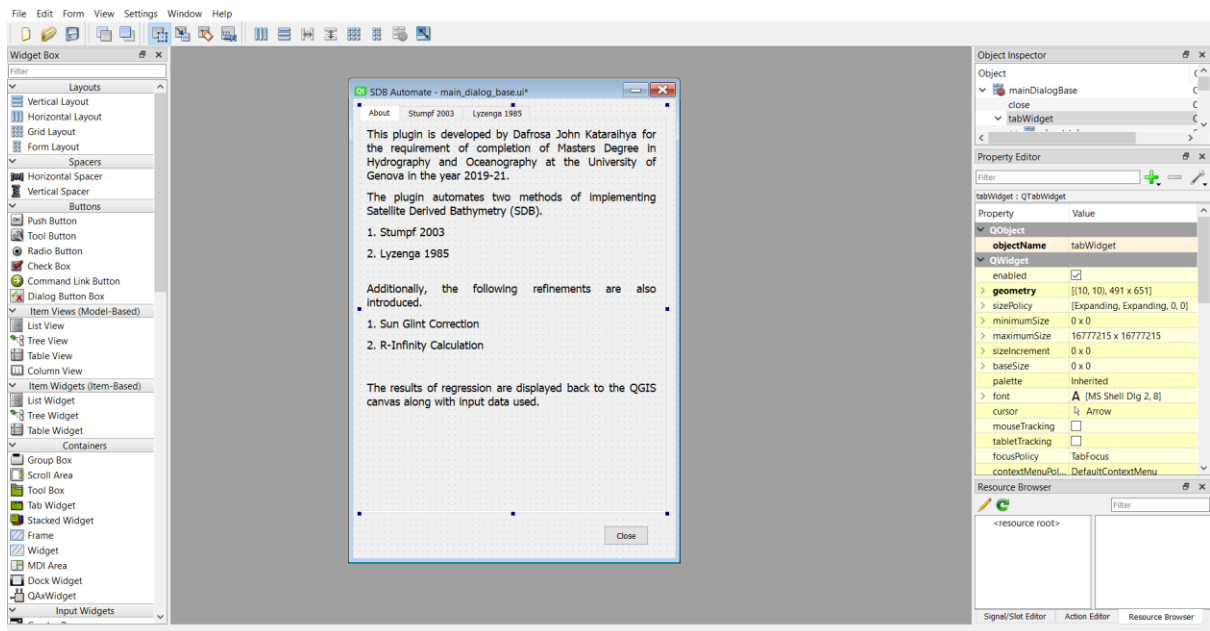


Figure 8: Creation of the plugin's user interface in Qt designer

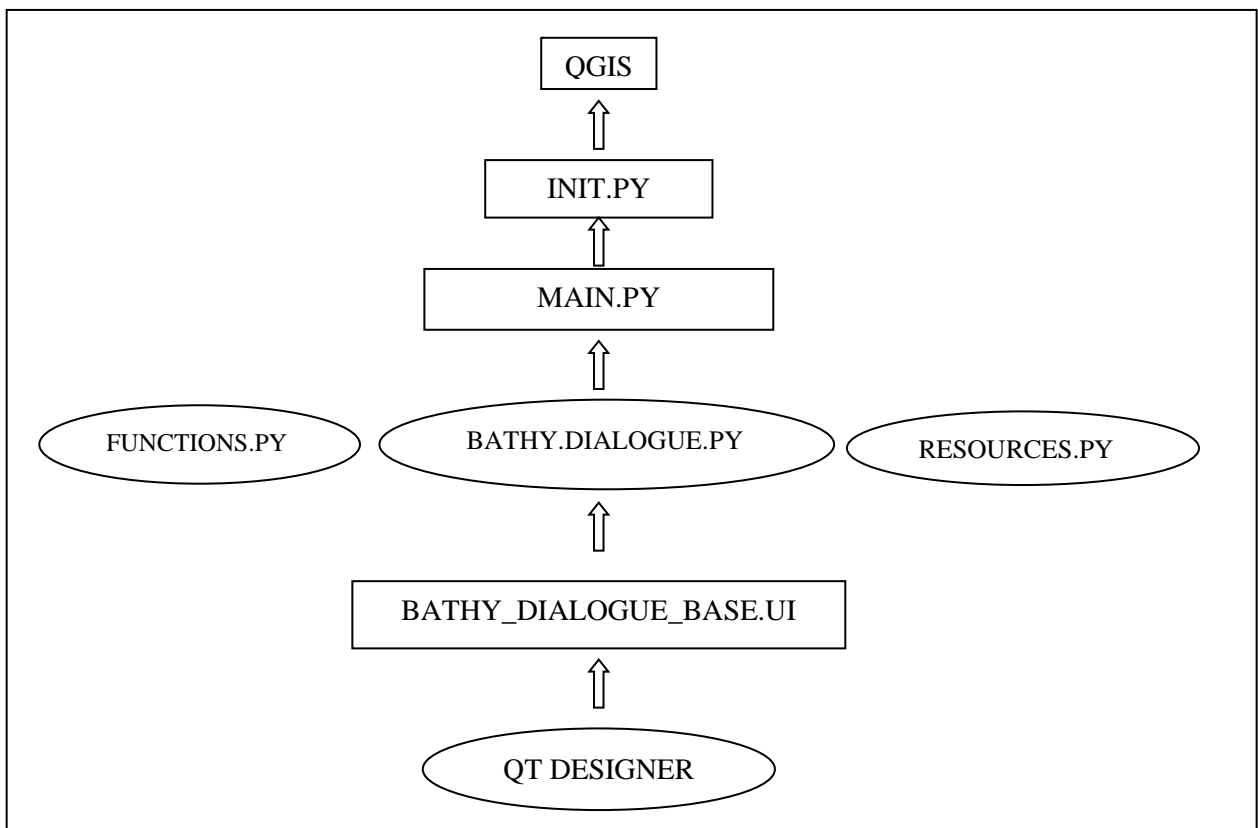


Figure 9: Diagram elaborating the internal structure of the plugin and how each file is linked until its representation in QGIS.

3.2.IMPLEMENTATION OF SDB ALGORITHM IN ‘SDB AUTOMATE PLUGIN’

The ‘SDB Automate Plugin’ functionalities are

- Separating the land and water area
- Sun glint correction
- Applying the Stumpf algorithm with different regression methods
- Applying Lyzenga algorithm workflow using different bands with a multiple linear regression (MLR)
- Deriving depths at region of interest

3.2.1. Delineating the water area

Once an image is collected, it may contain both land and water area. Since the plugin deals with determining bathymetry, only the water area is needed for processing. This is implemented by applying various spectral indices which are Normalized Difference Water Index (NDWI) or Modified Normalized Difference Water Index (MNDWI).

Normalized Difference water Index (NDWI)

Normalized Difference Water Index (NDWI) is a technique developed to delineate water features and heighten their presence in remote sensed images. The technique was invented in 1996 by McFeeters. It detects and analyses how the radiations from the sun interact with water molecules by using two spectral bands i.e., the Near Infrared (NIR) and the green bands. The NIR band is highly absorbed in water, while the green band is highly reflected hence enhancing the presence of any features available within the vicinity while eliminating the presence of land i.e., terrestrial vegetation features and soil. Equation below explains it where $L_{obs}(\lambda g)$ is Raster values observed in the green band and $L_{obs}(\lambda nir)$ is raster values observed in the NIR band.

$$NDWI = \frac{L_{obs}(\lambda g) - L_{obs}(\lambda nir)}{L_{obs}(\lambda g) + L_{obs}(\lambda nir)}$$

Modified Normalized Difference Water Index (MNDWI)

MNDWI is a modification of NDWI which was developed by (Xu 2006) it utilizes the Mid Infrared Band, the midinfrared band is within the range of 1550 to 1750 nm corresponds to the SWIR band within the range of 1560 to 1.660 nm. Hence the Short-Wave Infrared (SWIR) band is used instead of the NIR band. This enhances quality in extracting water information

from a region dominated by noise from built up land area or terrestrial vegetation. This technique is applicable for remotely sensed images which have the SWIR band. Equation ... explains MNDWI where $L_{obs}(\lambda_g)$ is reflectance observed in the green band and $L_{obs}(\lambda_{swir})$ is reflectance observed in the SWIR band.

$$MNDWI = \frac{L_{obs}(\lambda_g) - L_{obs}(\lambda_{swir})}{L_{obs}(\lambda_g) + L_{obs}(\lambda_{swir})}$$

3.2.2. Stumpf algorithm as implemented in the plugin

Stumpf algorithm as described by the IHO cookbook (2019) uses the log ratio method. It utilizes the green and blue bands for depth derivation while using red and NIR bands for land/sea separation. Unlike the normal Stumpf workflow, ‘SDB Automate plugin’ figure 10 has included more regression methods i.e., linear, log and polynomial for further depth derivation during the vertical referencing stage.

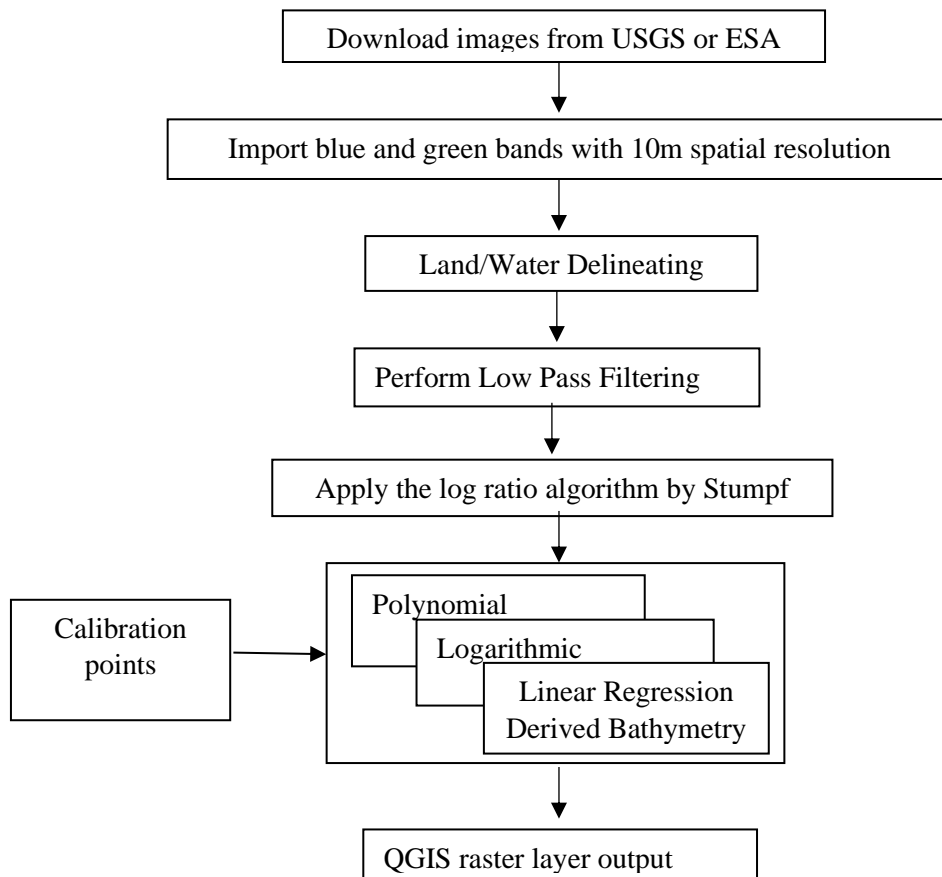
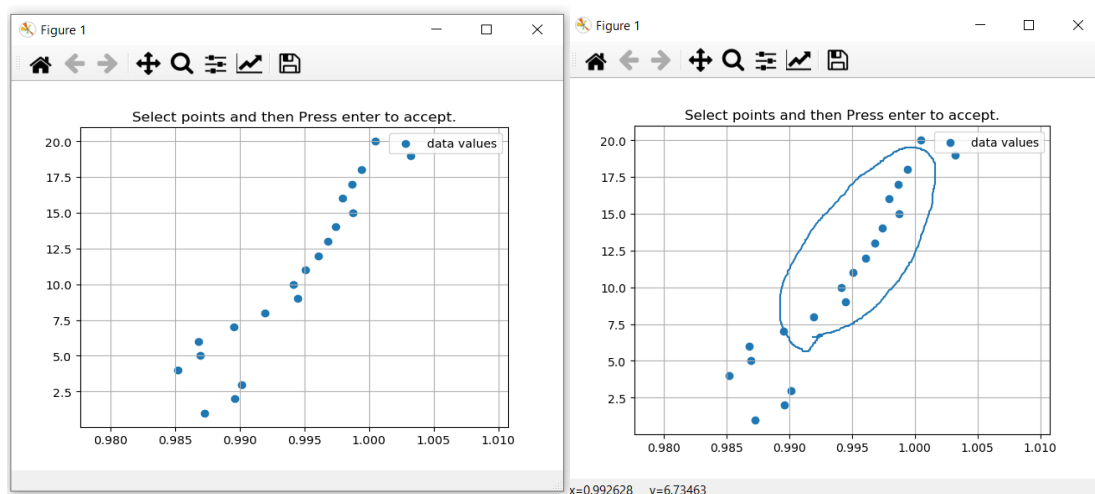


Figure 10: Diagrammatical representation of the Stumpf algorithm workflow as implemented in the plugin

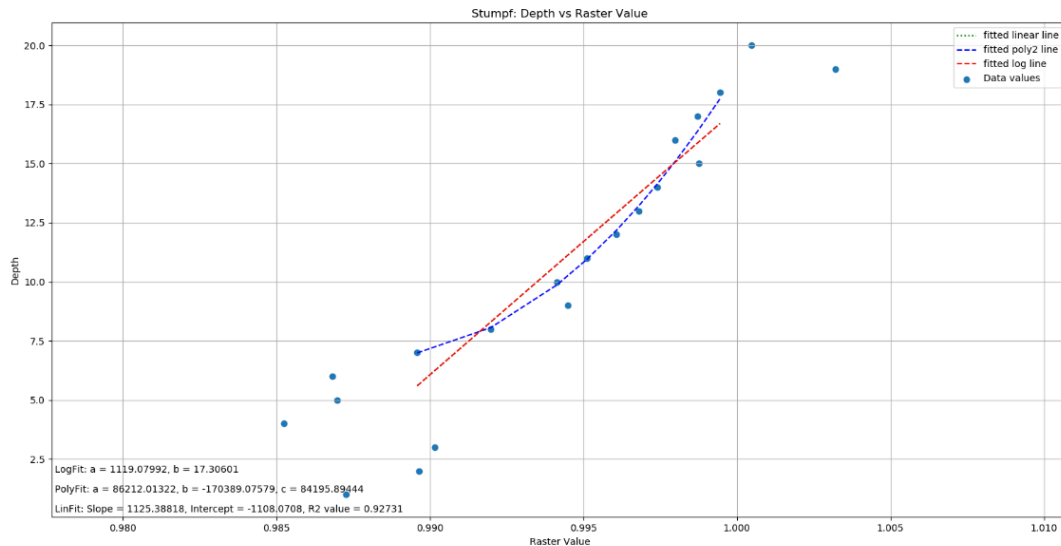
The guidelines for deriving bathymetry from satellite as described in the IHO cookbook 2019 are:

- i. Downloading of satellite images considering the geographical location, extent of cloud cover and level of pre-processing, the weather conditions on the date of data acquisition. Images with a pronounced turbidity, suspended particulate matter are not encouraged as would lead to bad results. Images were downloaded from USGS website.
- ii. Spatial filtering. This is done in order to eliminate random fluctuations of spectral signatures during data collection. Different filters can be applied depending on the available data and the ultimate use.
- iii. Water delineation, this was done using two different water indices i.e., NDWI and MNDWI as explained in chapter 2.
- iv. Identifying the area for depth extraction depending on the intended Region of interest (ROI) and the available hydrographic data.
- v. Application of the Stumpf algorithm. The bathymetry was calculated using the green and blue bands.
- vi. Vertical Referencing. A linear regression between the green and blue band against the calibration points /depth values is attained. For this thesis, linear, log and polynomial regressions were applied to analyse which regression yielded better results. During this process, the user interacts with the software to enable perfect selection of the distribution of points for the regression line creation (fig 11).



(a)

(b)



(c)

Figure 11: Narrates on the vertical referencing (a) display of the regression points where the user selects the points in relative to the distribution (b) the selection process (c) the display of all the regression lines created i.e., linear, log and polynomial.

This is the general outlook of the plugin in QGIS when processing the Stumpf algorithm.

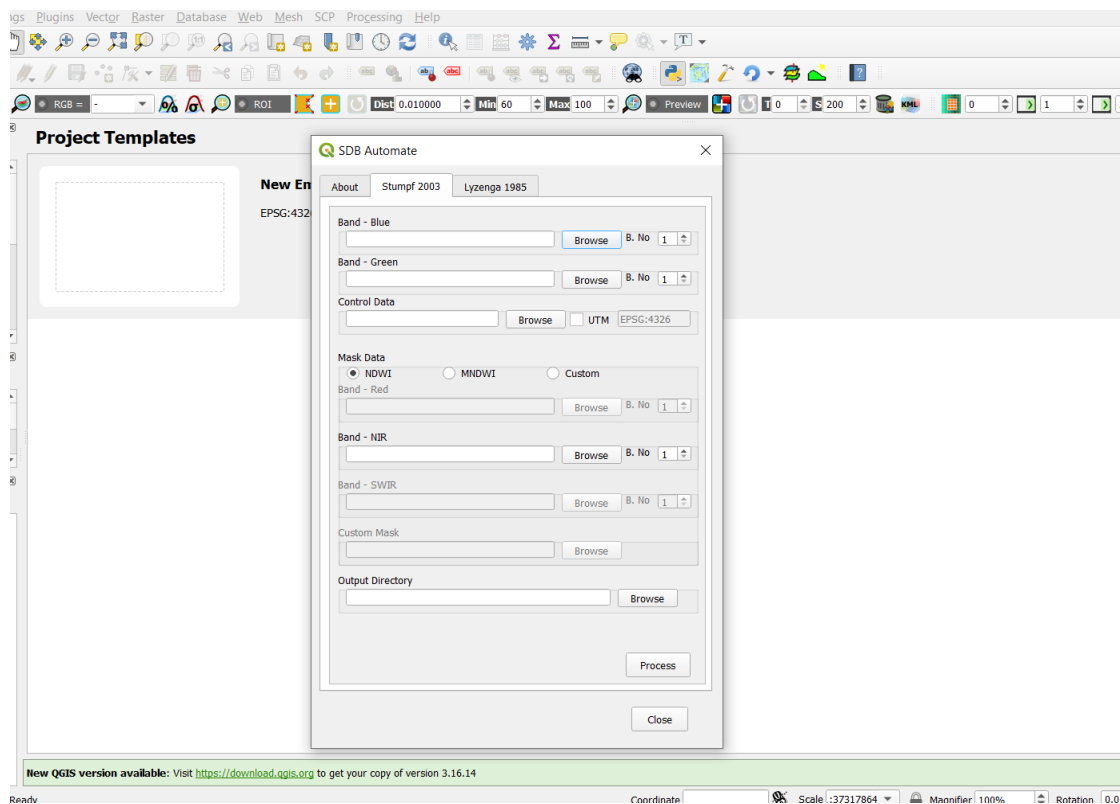


Figure 12: Plugin user interface presentation while running the Stumpf algorithm as is displayed for use in QGIS

3.2.3. Lyzenga algorithm as implemented in the plugin

Lyzenga 1985, elaborates on how different multispectral bands can be utilized to obtain bathymetry. The spectral bands used are green, red, blue and blue aerosol from both Sentinel 2 and Landsat 8 for depth determination while the NIR plus red was used for land/sea separation. Lyzenga's workflow follows the same workflow as Stumpf in the first four steps but from the fifth it changes to accommodate the Lyzenga algorithm.

The Lyzenga workflow as implemented in the plugin:

- i. Consider steps 1 through 5 in the Stumpf workflow but with more bands
- ii. Data pre-processing by applying the sun glint correction. As elaborated in chapter 2 of this thesis.
- iii. Depth calibration by extracting the deep-water areas, the plugin generates a true colour image (fig 12) which allows the user to interact with the plugin by carefully selecting the deep area in the image. The area selected is masked over all bands to determine the deep area reflectance (L_{si}). These values are used to calibrate the $X = \ln(L_i - L_{si})$, raster values for each respective band used.
- iv. Vertical referencing by performing the Multiple linear regression using the calibration points and the X variables for each band pair.

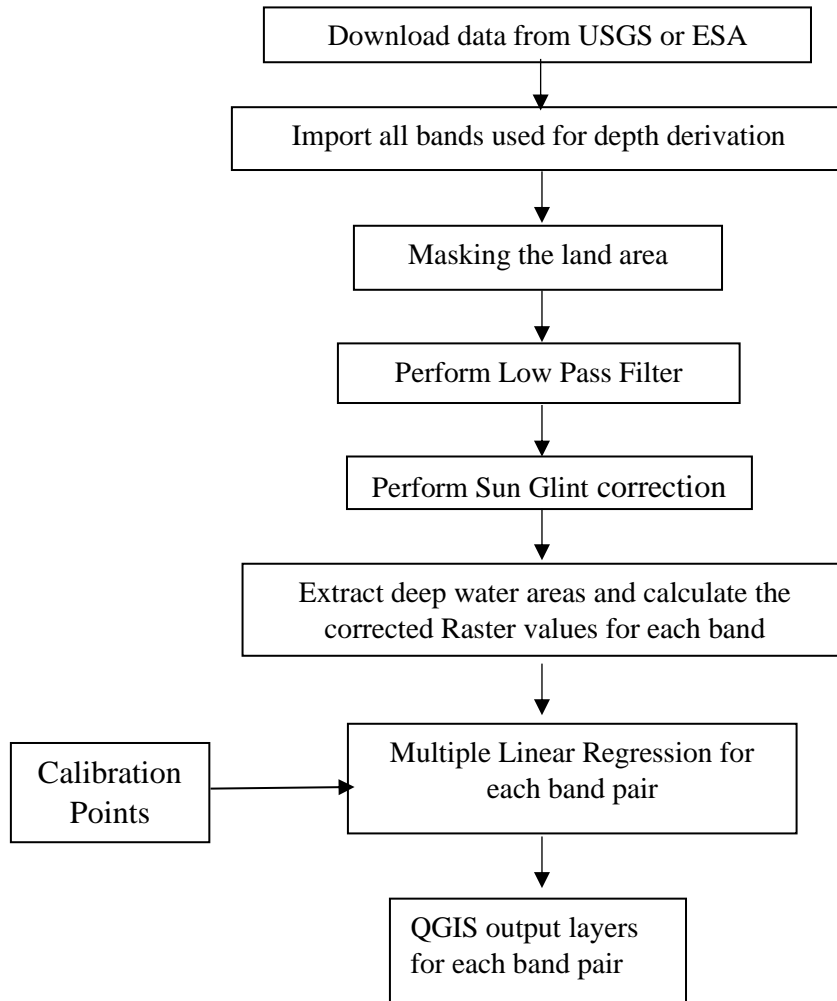


Figure 13: Lyzenga algorithm workflow as implemented in the plugin

The interface of the Lyzenga algorithm is seen in figure 14 as implemented in the plugin. It is a must to import the green, blue and red band for the Lyzenga workflow to work.

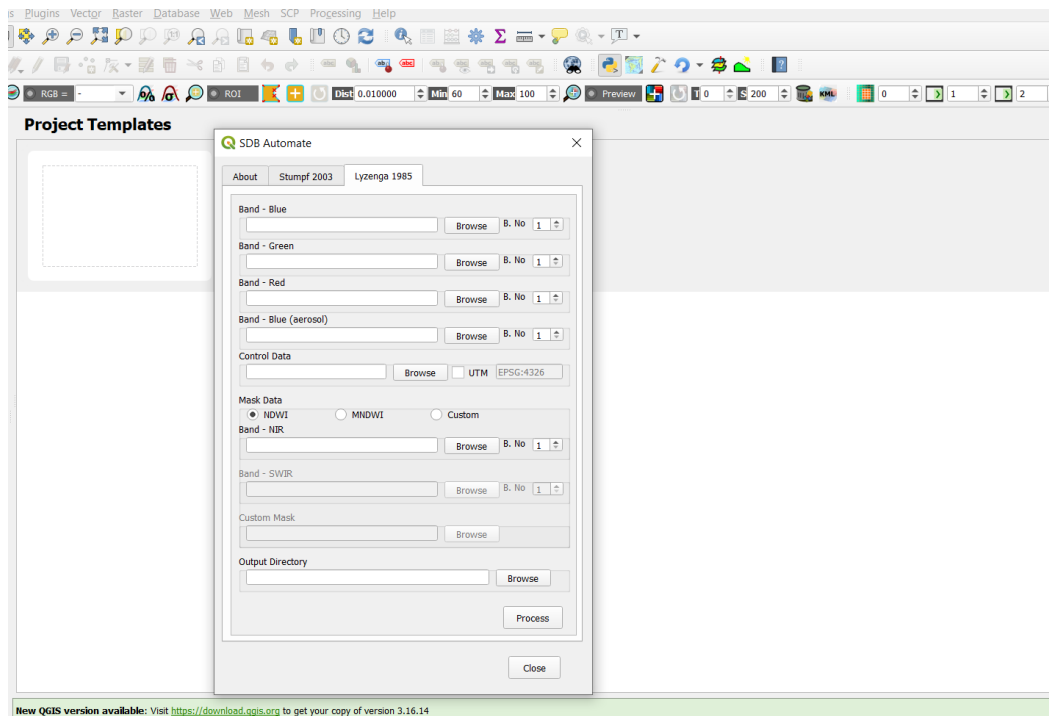


Figure 14: Plugin user interface presentation while running the Lyzenga algorithm as is displayed for use in QGIS

It should be noted that for control/calibration points file, either shapefiles (.shp) or text (.txt)/(.csv) formats can be imported in the plugin. If (.txt/ .csv) format is used and is in projected coordinates reference system, one is supposed to flag the UTM box and identify the respective EPSG code. If geographic coordinate reference system is used, user should not flag the UTM box.

Also, for both algorithms, the plugin made sure to divide the control points into two groups in an 80/20 ratio. Where 80% of the control points were used for calibration while 20% were used for checking.

3.3.RESEARCH AREA AND DATA

3.3.1. Research Area

The area along the coast of La Spezia and Livorno was chosen due to its nature. It is shallow area along the Western coast of Italy in the Tyrrhenian Sea (figure 15). It being a shallow area, the normal hydrographic techniques cannot be used to survey the area intensively since the area imposes a danger to navigation hence can lead to destruction of instruments used.

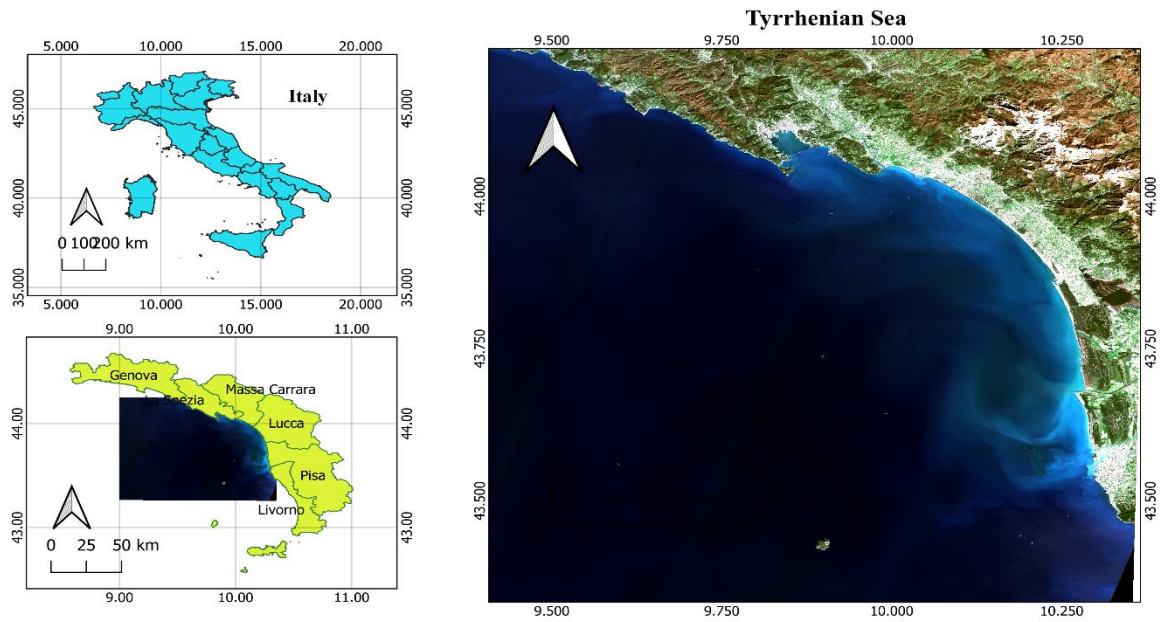


Figure 15: Map depicting the study area

3.3.2. Data

This thesis considered the use of two kinds of data

i. The control and calibration data

This data was manually digitized from electronic navigational charts (ENC) obtained from the Hydrographic Institute of the Italian Navy. The ENC (figure 16) used were *IT300003* & *IT300004* which had a scale of 1:100000 and *IT400115* & *IT4000120* with a scale of 1:30000.

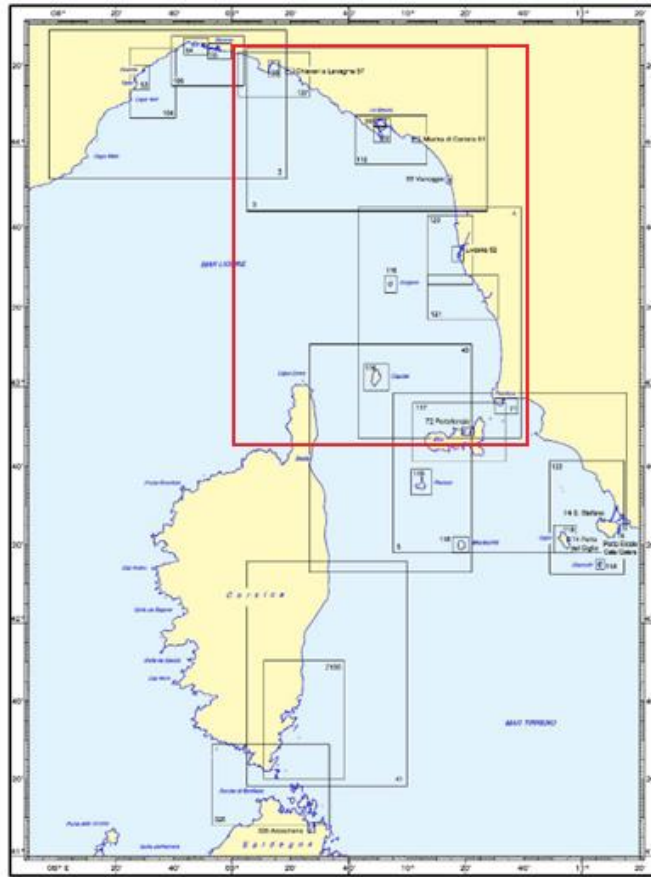


Figure 16: Electronic Navigation Chart (ENC) tiles in red, used for validating the tool.

- ii. Freely available sentinel 2A Multi Spectral Imaging mission (MSI) satellite images from the USGS earth explorer website <https://earthexplorer.usgs.gov/>, downloaded at 10m spatial resolution (table 1), with Level 1C pre-processing level. Images were chosen considering the cloud cover, surface waves, sediment plumes and sun glint. The images covered three (3) years i.e., 2017, 2018 and 2019.

Date Range
Cloud Cover
Result Options

Search from: to:
 Search months: (all)

Data Sets »
Additional Criteria »
Results »

(a)

Date Range
Cloud Cover
Result Options

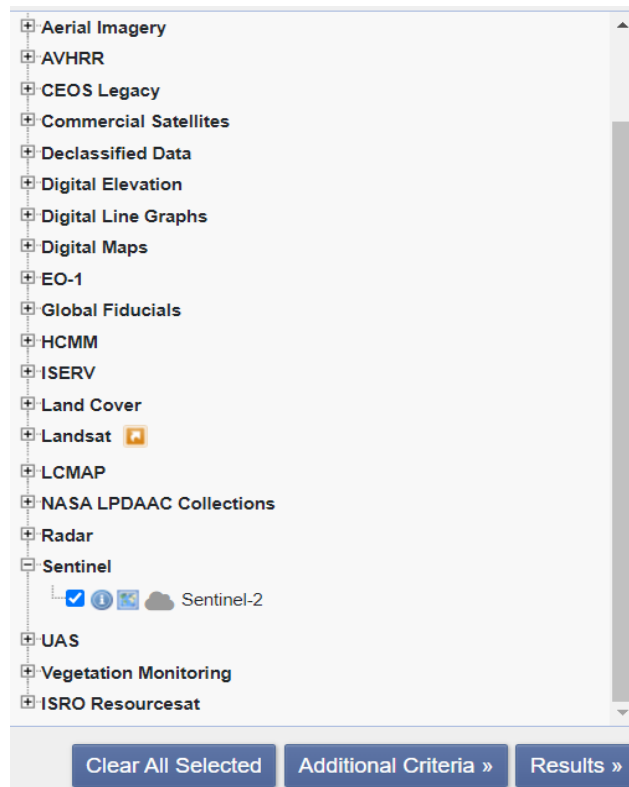
Cloud Cover Range: 0% - 15%

Unknown Cloud Cover Values Included

This filter will only be applied to data sets that support cloud cover filtering (● in the data set list denotes cloud cover support).

Data Sets »
Additional Criteria »
Results »

(b)



(c)

Figure 17: (a), (b), (c) depicting the image selection and downloading process

Table 1: Satellite Images used in the plugin

Satellite	Pre-processing level	Acquisition date	Spatial Resolution
Sentinel 2A	Level 1C	03/07/2017	10m
Sentinel 2A	Level 1C	19/05/2018	10m
Sentinel 2A	Level 1C	13/07/2019	10m

iii. SDB Algorithm implementation, band pairs and regression relationships.

Lyzenga algorithm was implemented using the green, blue and red bands of satellite images. Blue-red combination and green-red combination following (Gao, 2009) suggested a shift to long wavelengths on areas with increased turbidity hence the use of the red band.

Table 2: Summary of SDB algorithms used and the band pairs

SDB Algorithm	Bands Used	Regression Relationship
Lyzenga	Blue- Green	Multiple Linear regression
	Blue- Red	Multiple Linear regression
	Green- Red	Multiple Linear regression
Stumpf	Blue- Green	Linear
	Blue- Green	Exponential
	Blue- Green	2 nd Order polynomial

3.4.VALIDATION OF THE PLUGIN

3.4.1. Pre-Processing

Control and check data was sorted to a range of 1.5m to 12m since it contained data at very deep areas. The data that was below or above that range was eliminated. This was done using the simple sorting tools in excel. A total of 791 points were used.

After observing that the control points were mostly concentrated at two main areas (figure 18) i.e., IT400115 and IT400120 spaced every after 300 metres, it was decided that, for better SDB results, it is best to slice the images into two areas which are filled with control points while maintaining the same resolution of the satellite images.

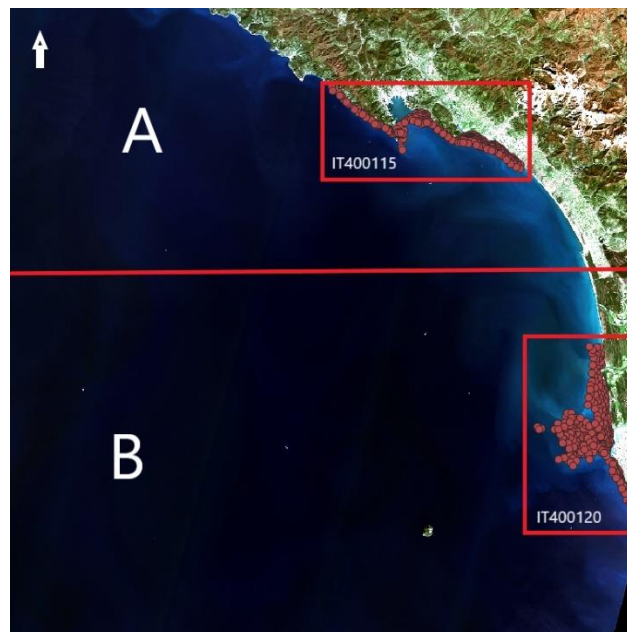


Figure 18: Distribution of control points based on IT400115 &IT400120 ENCs, and the red line indicating the slicing area of the image into image A (La Spezia) and image B (Livorno).

3.4.2. Stumpf Validation

After importing the required images in the plugin (figure 19), the following results were obtained from the Stumpf algorithm.

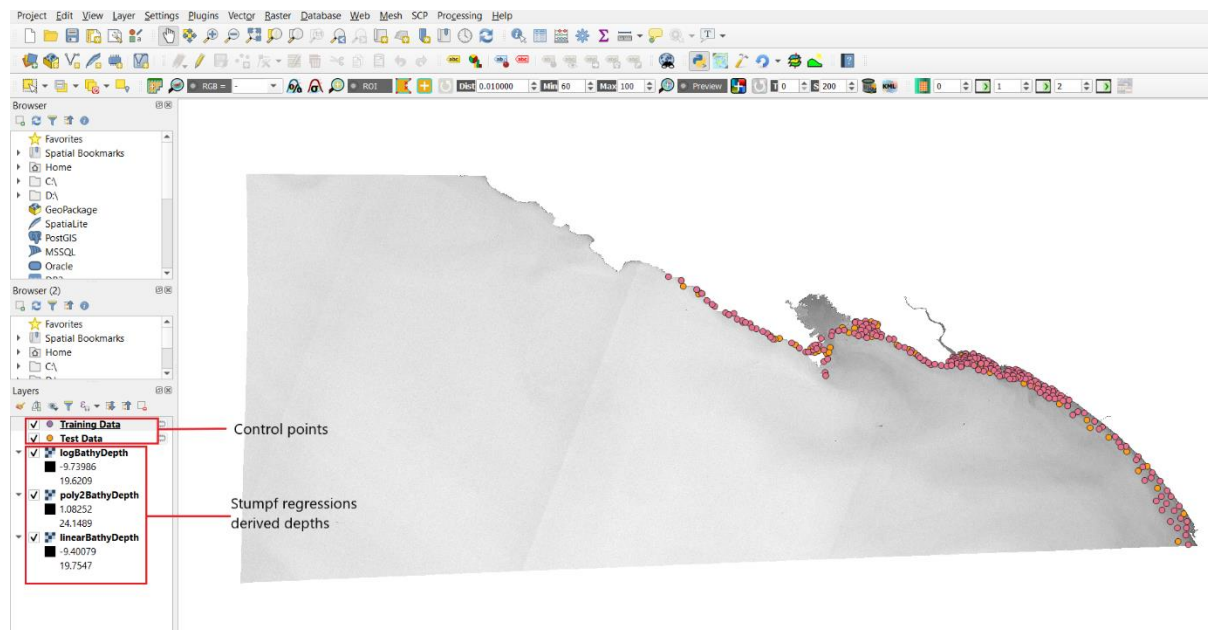


Figure 19: Final output display while running the Stumpf algorithm.

Vertical referencing is among the important procedures in obtaining bathymetry using the empirical approach. This is where utmost attention is needed since the user is required to carefully analyse the trend between actual depth from ground control points against the ratio of the blue and green band in order to determine the gain and offset.

In order to validate this plugin, gain and offset were calculated, figures 20 shows the generated graphs under Stumpf workflow in all three regressions used in 2017, 2018, 2019 divided into two regions i.e., A (La Spezia) and B (Livorno).

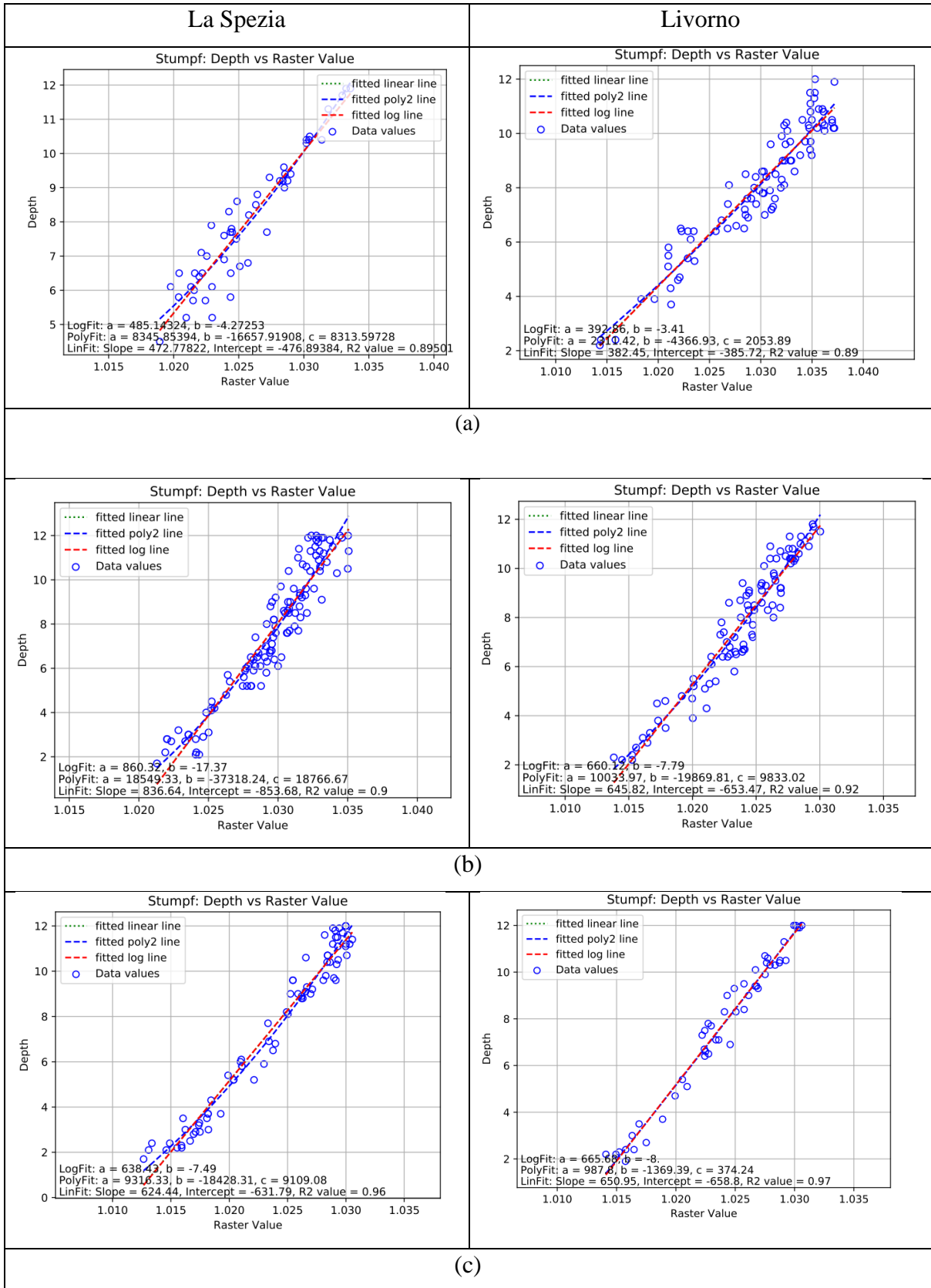
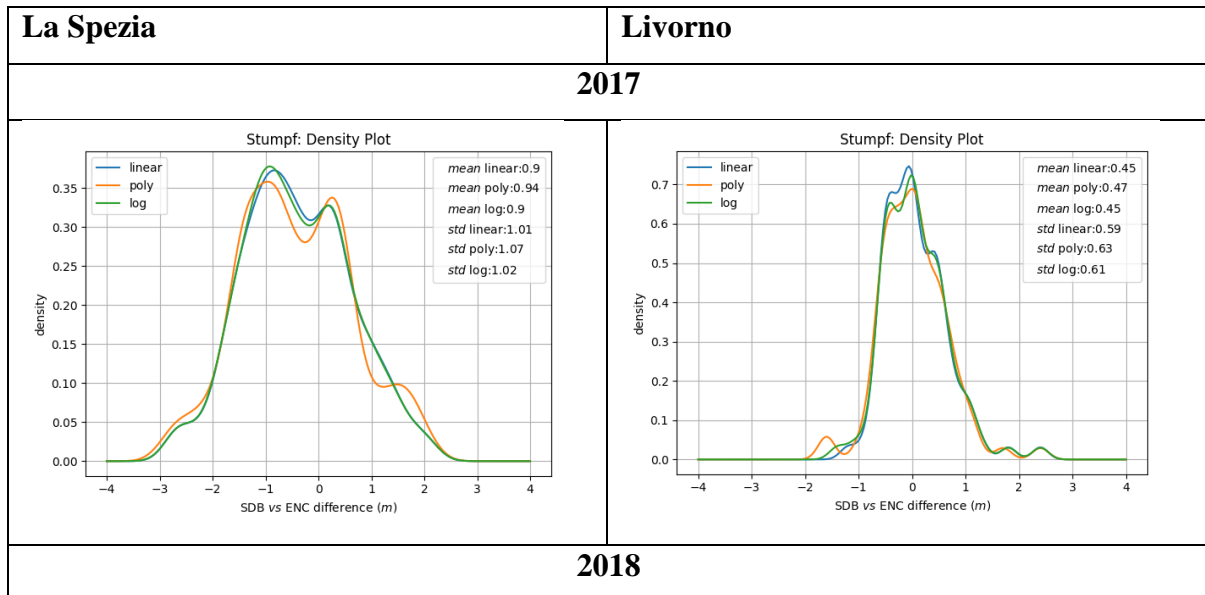


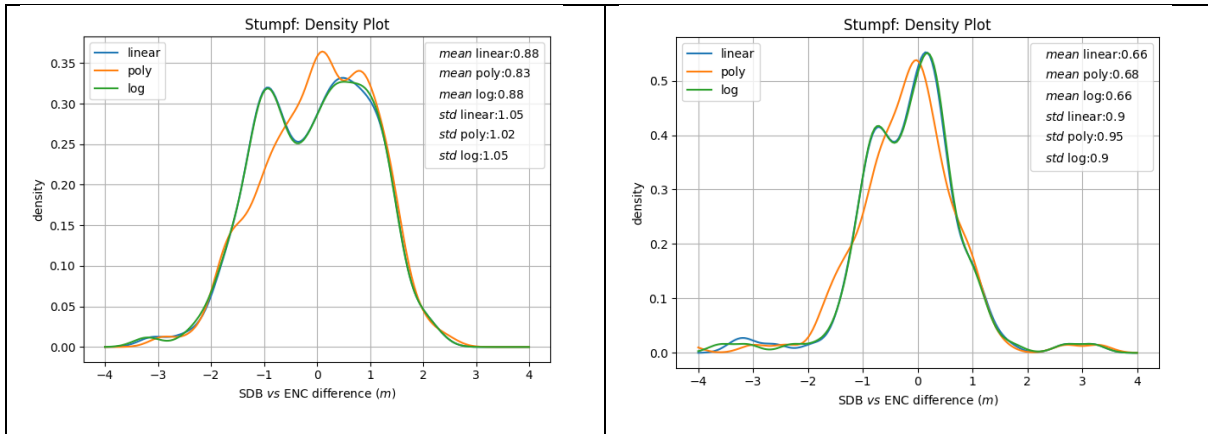
Figure 20: (a)-2017, (b)-2018, (c)-2019, calculating the gain and offset using the control points and the ratio between blue and green band (raster value)

Table 3: Values obtained in vertical Referencing

Regression	2017		2018		2019	
Spezia						
	Gain	Offset	Gain	Offset	Gain	Offset
Linear	472.78	-476.89	836.64	-853.68	624.44	-631.79
Logarithmic	485.14	-4.27	860.32	-17.37	638.43	-7.49
2 nd order polynomial	a = 8345.85, b = -16657.92, c = 8313.6		a = 18549.33, b = -37318.24, c = 18766.67		a = 9316.33, b = -18428.31, c = 9109.08	
Livorno						
Linear	382.45	-385.72	645.82	-653.47	650.95	-658.8
Logarithmic	392.86	-3.41	660.12	-7.79	665.68	-8.55
2 nd order polynomial	a = 2311.42, b = -4366.93, c = 2053.89		a = 10033.97, b = -19869.81, c = 9833.02		a = 987.8, b = -1369.39, c = 374.24	

Graph 1: Kernel Density charts portraying how much the SDB varies compared to the ENC's actual depth following the Stumpf workflow. Charts were created using the Python (matplotlib). All graphs are right skewed with the standard deviation indicating a generally low spread of values.





2019

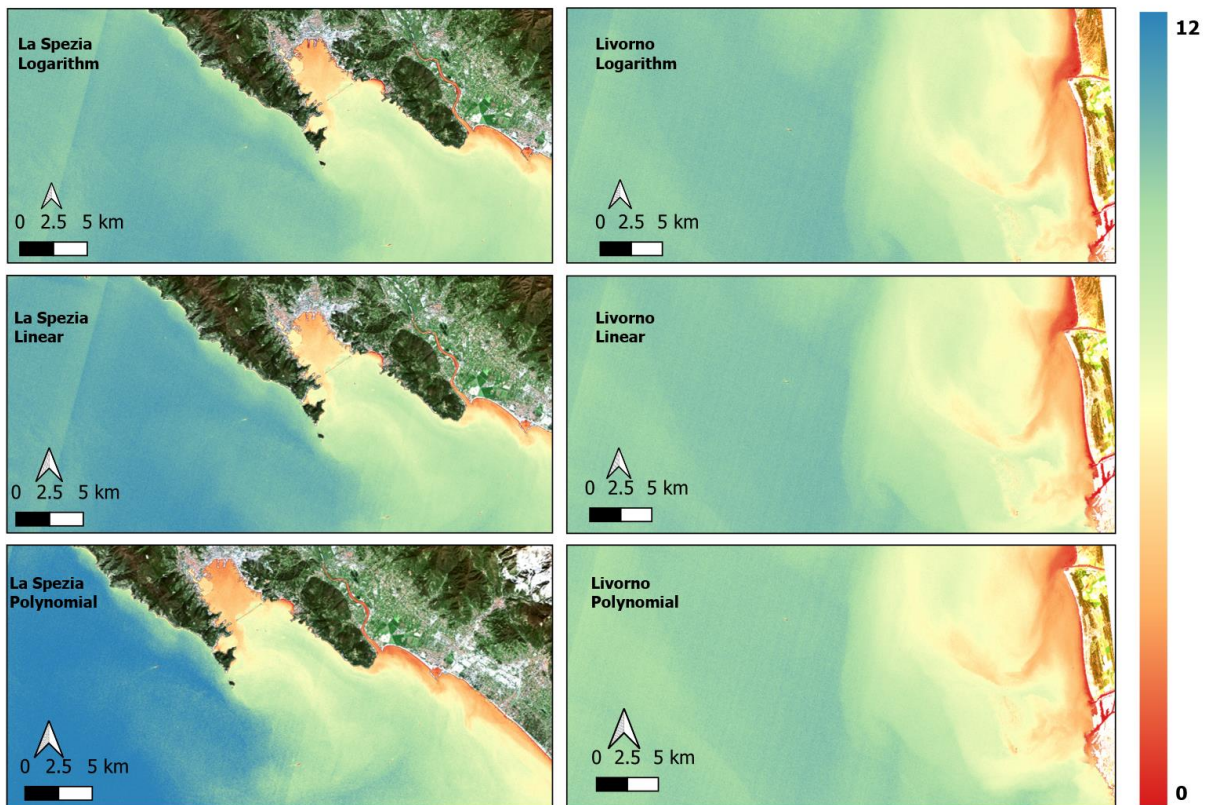
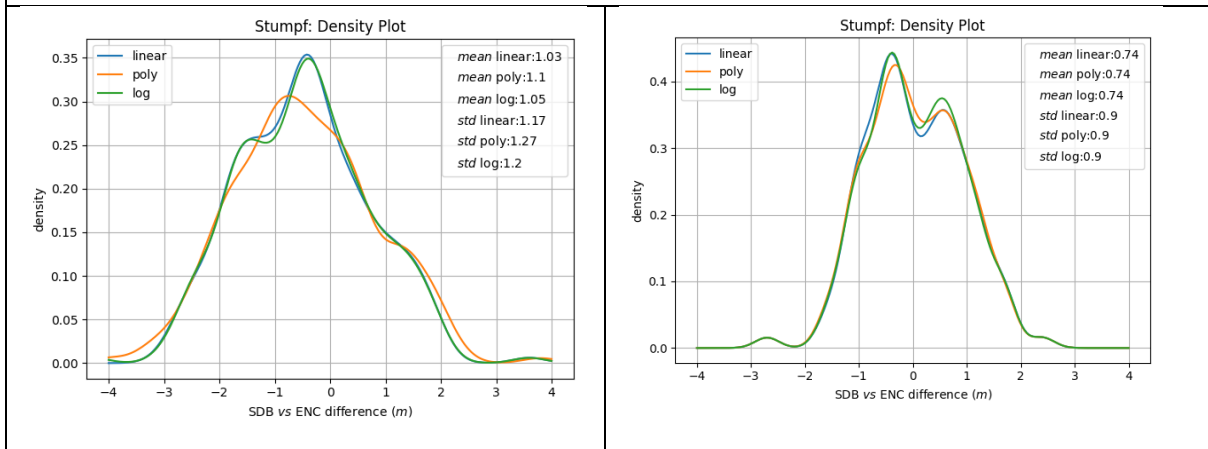


Figure 21: Sample of Stumpf SDB variants derived from Sentinel-2 imagery for La Spezia (L.H.S) and Livorno (R.H.S) for 2017, colour ramp indicates the depth variation.

3.4.3. Lyzenga validation

While implementing the Lyzenga workflow, determination of the deep area in order to calculate for $X = \ln(L_i - L_{si})$ of each band used is a crucial part. After generating these values, multiple linear regression is performed using two band pairs in order to generate depth.

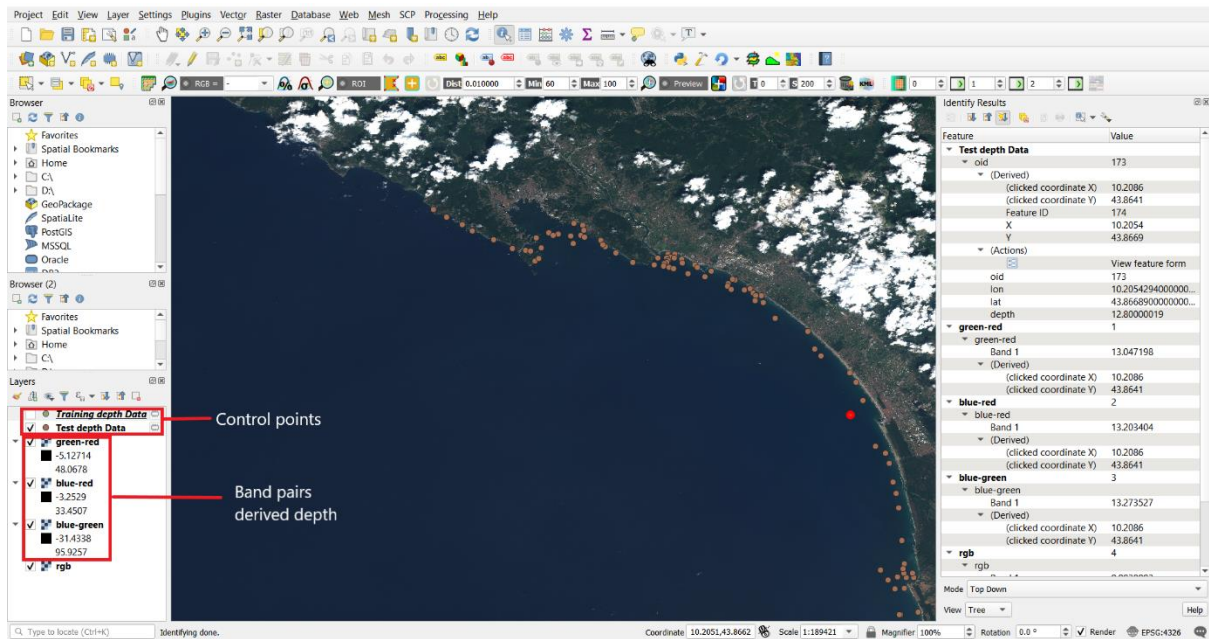
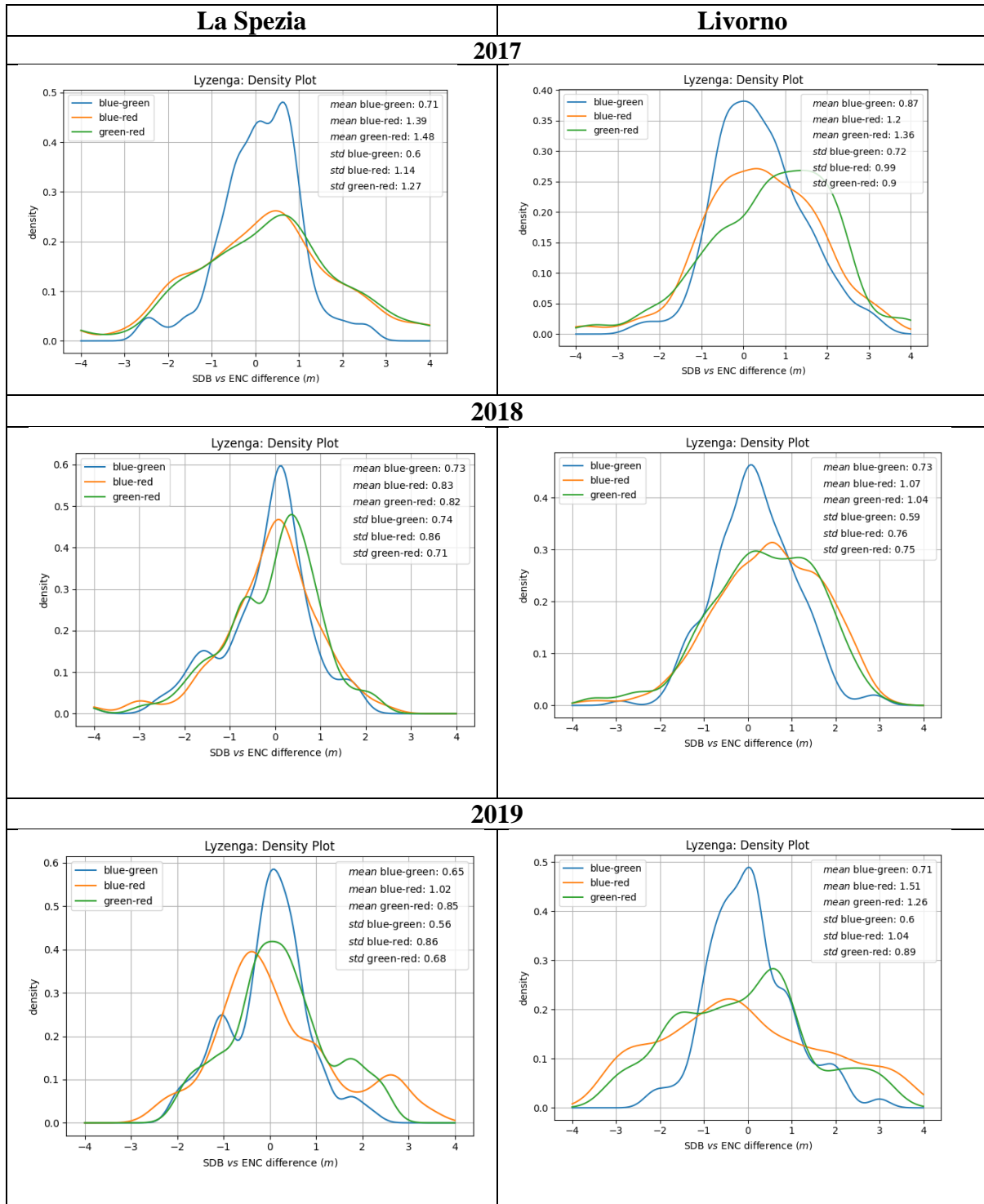


Figure 22: Final output display using Lyzenga algorithm

After obtaining the depth values (figure 22), the test data (20% of the whole dataset) was used for checking. Root Mean Square Error (RMSE: average difference with the ground truth points), R^2 values (indicating how well the SDB algorithms fit their trendlines (graph 2, tables 5&6) and error range (full range difference with the ground control points) was determined.

Graph 2: Kernel Density charts portraying how much the SDB varies compared to the ENC's actual depth following the Lyzenga workflow. Charts were created using the Python (matplotlib). All graphs are right skewed with the standard deviation indicating a generally low spread of values.



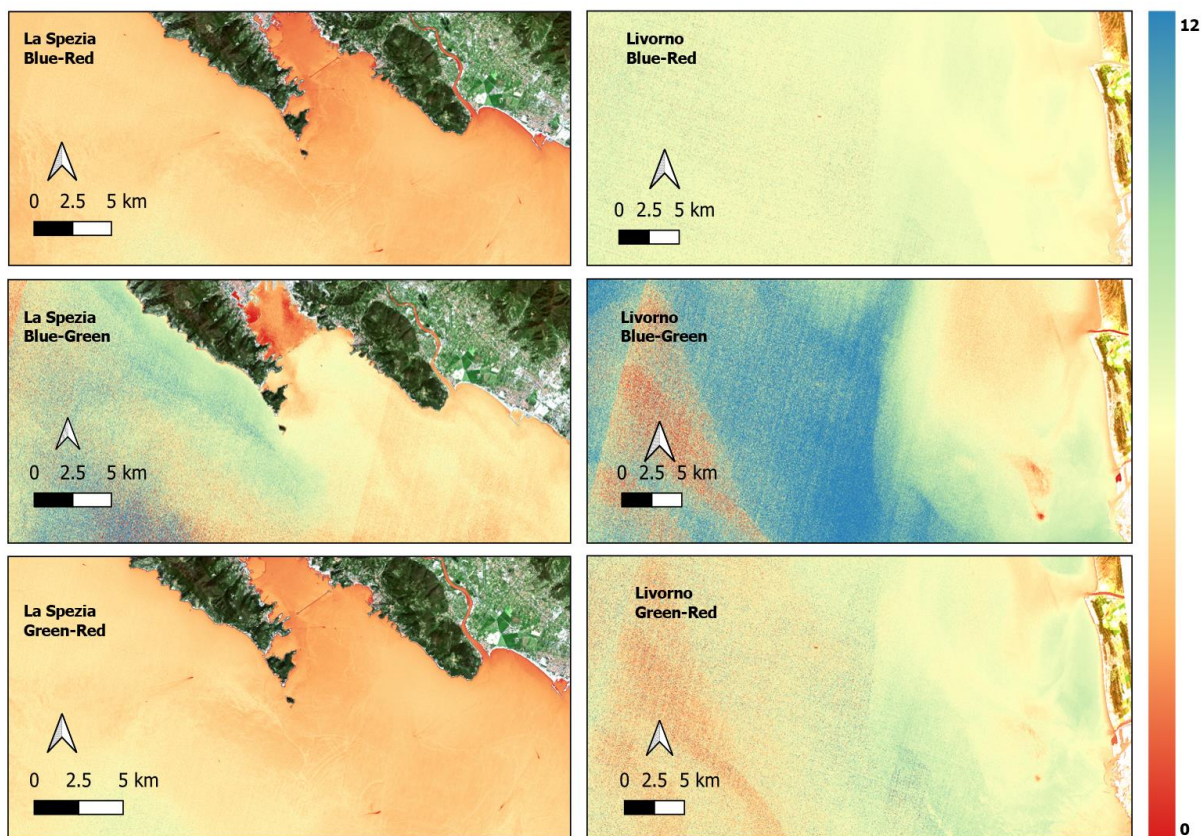


Figure 23: Sample of Lyzenga SDB variants derived from Sentinel-2 imagery for La Spezia (L.H.S) and Livorno (R.H.S) for 2017 colour ramp indicates the depth variation.

Table 4: Multiple Linear regressions coefficients for each band pair of 2017, 2018 and 2019 images at La Spezia and Livorno.

SDB Variants	Intercept	Coefficient 1 st band	Coefficient 2 nd band
LA SPEZIA			
2017			
MLR of Blue-green band	34.501	1.572	-5.543
MLR of Red-Blue band	20.261	0.1038	-2.887
MLR of Green-Red band	21.479	-0.225	-2.766
2018			
MLR of Blue-green band	33.040	0.898	-5.358
MLR of Red-Blue band	19.622	-0.081	-2.317
MLR of Green-Red band	31.491	-4.773	0.561
2019			
MLR of Blue-green band	39.371	1.909	-7.283
MLR of Red-Blue band	21.607	-0.061	-2.653
MLR of Green-Red band	30.059	-2.936	-1.082
LIVORNO			
2017			
MLR of Blue-green band	20.1139	10.1081	-10.4601
MLR of Red-Blue band	19.7135	3.2135	-3.3859
MLR of Green-Red band	9.249	1.007	-1.7158
2018			
MLR of Blue-green band	24.2457	9.2915	-11.7501
MLR of Red-Blue band	20.4515	2.2069	-4.5264
MLR of Green-Red band	16.593	-3.8197	2.3202

2019			
MLR of Blue-green band	29.924	14.7229	-18.07688
MLR of Red-Blue band	36.0097	-0.1066	-5.2563
MLR of Green-Red band	34.0794	-4.3777	-0.4035

Table 5: SDB algorithm performance: Root Mean Square Error (RMSE: average difference with the ground truth points), R^2 values (indicating how well the SDB algorithms fit their trendlines and error range (full range difference with the ground control points) at La Spezia.

SDB Variants	R^2 (m)	RMSE (m)	Range (m)
Stumpf			
2017			
Linear	0.88	1.06	0.897
Log	0.87	1.09	0.901
2 nd order polynomial	0.88	1.14	0.942
2018			
Linear	0.89	1.08	0.883
Log	0.89	1.07	0.881
2 nd order polynomial	0.89	1.01	0.891
2019			
Linear	0.86	1.26	1.034
Log	0.85	1.29	1.046
2 nd order polynomial	0.84	1.35	1.102
Lyzenga			
2017			
MLR of Blue-green band	0.87	0.92	0.708
MLR of Red-Blue band	0.54	1.79	1.393
MLR of Green-Red band	0.46	1.94	1.481
2018			
MLR of Blue-green band	0.85	1.04	0.731
MLR of Red-Blue band	0.8	1.19	0.832
MLR of Green-Red band	0.84	1.08	0.824
2019			
MLR of Blue-green band	0.92	0.85	0.65
MLR of Red-Blue band	0.82	1.32	1.021
MLR of Green-Red band	0.88	1.08	0.85

Table 6: SDB algorithm performance: Root Mean Square Error (RMSE: average difference with the ground truth points), R^2 values (indicating how well the SDB algorithms fit their trendlines and error range (full range difference with the ground control points) at Livorno.

SDB Variants	R^2 (m)	RMSE (m)	Range (m)
Stumpf			
2017			
Linear	0.95	0.59	0.445
Log	0.95	0.61	0.455
2 nd order polynomial	0.95	0.62	0.471

2018			
Linear	0.90	0.90	0.657
Log	0.90	0.91	0.656
2 nd order polynomial	0.89	0.96	0.68
2019			
Linear	0.93	0.87	0.742
Log	0.92	0.84	0.736
2 nd order polynomial	0.82	0.86	0.938
Lyzenga			
2017			
MLR of Blue-green band	0.77	1.13	0.872
MLR of Red-Blue band	0.57	1.55	1.2
MLR of Green-Red band	0.53	1.62	1.356
2018			
MLR of Blue-green band	0.83	0.93	0.728
MLR of Red-Blue band	0.67	1.30	1.068
MLR of Green-Red band	0.68	1.28	1.044
2019			
MLR of Blue-green band	0.88	1.00	0.747
MLR of Red-Blue band	0.57	1.94	1.579
MLR of Green-Red band	0.72	1.57	1.284

4. CHAPTER FOUR: DISCUSSION AND RESULTS ANALYSIS

4.1.PLUGIN WORKING ENVIRONMENTS

The developed tool proved to work efficiently with different kinds of multispectral images e.g., Sentinel 2 images at different spatial resolution.

Same dataset was run between 2 computers with different specifications.

Table 7: Plugin working environments and time used while processing SDB algorithms

	Computer 1	Computer 2
RAM	16 GB	32 GB
Operating System (OS)	Ubuntu	Windows
Stumpf Processing Time	Approx. 3minutes	Approx. 2minutes
Lyzenga Processing Time	10-12minutes	7-10 minutes

With the observation in Table 7 above, the plugin takes the shortest time when using a powerful computer i.e., computer 2. But generally, the plugin works for computers with a minimum of 8GB RAM and in any OS.

4.2.SATELLITE DERIVED BATHYMETRY

Both algorithms gave good results as analysed in table 5 & 6 above.

4.2.1. Stumpf workflow Results

- Figures 20, shows the vertical referencing process. The process yields the tuneable constants for values for all the regression coefficients for depth generation. Data was analysed in order to obtain the best regression values for depth derivation.
- The linear and logarithm regressions show almost similar results for the same area and data as observed in graph 1, 2nd order polynomial gives slightly different results when compared to the actual depth. It was further observed that, 2nd order polynomial can be used to analyse deep areas since it can compensate for the nonlinear relationship between the actual depth and the raster values.
- The areas close to the coast around 1-3metres deep, areas close to barriers (around the port area or water breakers) did not show a good correlation due to strong water mixing caused by waves.

The mean error for the Stumpf workflow ranges between 0.5m to 1.2m.

Generally, for better results, it is important to have

- Equally distributed and closely spaced control data for model training. The degree of how good the data is, is dependent on the distribution and accuracy of the control data.
- Since the accuracy is dependent on the control data, it is important to limit the extent of the raster image coverage in accordance with the control data coverage as how it was implemented in this thesis i.e., slicing the image to fit the available control data.

4.2.2. Lyzenga Workflow Results

Lyzenga workflow was tested using 3 bands i.e., Blue, Green and Red. And the bands gave good results with R^2 values for the blue-green band pair ranging between 0.77-0.95 as observed in Table 5 & 6. Blue and green band pairs gave better results as compared to the other band pairs.

At areas with pronounced water mixing, turbidity, river outlet or the port entrance, the band pairs between green and red, or blue and red, gave better results. This is because of the presence of suspended matter which changes the spectral composition and thus the spectral response on the satellite. Therefore, the Red Band is a perfect band to be paired with blue or green to determine depth at such areas.

The mean error in the Lyzenga workflow for all band pairs ranges from 0.65m to 1.6m.

4.2.3. Workaround of the Physics Approach to SDB

This thesis intended to further investigate the possibility of applying the Multiple Linear Regression Coefficients from the Lyzenga workflow to determine depth. Table 4 displays the MLR coefficients of both La Spezia and Livorno. As it can be observed from the three years i.e., 2017, 2018 and 2019, the coefficients appear to have relatively close values to each other.

The coefficients obtained in 2017, were used to calculate depth for the images in 2019 without solving the whole light propagation equation i.e., multiple linear regression was not implemented between the blue, green and red band. And thereafter, the obtained depth was compared to the actual depth. The results had an error range of about 1.9m to 2.5m.

This proves that for a specific area which is not very different in space and time, water characteristics behave similarly. Hence same coefficients can be applied to derive bathymetry without the need of control points.

5. CHAPTER FIVE: CONCLUSION AND RECOMMENDATION

5.1. Conclusion

Satellite Derived Bathymetry is indeed becoming extremely popular especially for areas which are not easily accessible while using the “in situ” methods. Satellites generate images at a very short temporal resolution, hence if frequent check is needed, images are always available.

Therefore, the generated tool can be considered as an effective solution to timely determining the SDB. The tool is available through local installation into the QGIS software.

All the case studies were aimed to evaluate the performance of the tool. The accuracy of SDB depends upon satellite images characteristics, number and distribution of calibration points and water conditions of the study area.

5.2. Recommendations

In order to fully refine the SDB methods, Geographically Weighted Regression can be implemented in the tool to enable inclusion of different geographical related aspects in SDB determination.

Also, the use of Support Vector Machine (SVM) as part of Machine Learning, this aids in training different algorithms/models through performing classification, regression and even outlier detection. Hence in the long run, control data won't be required when determining SDB but only the needed images.

REFERENCES

- D. R. Lyzenga, N. P. Malinas, F. J. Tanis. (2006). Multispectral bathymetry using a simple physically based algorithm. *IEEE Transactions on Geoscience and Remote Sensing*, 2251 - 2259.
- G. Doxani, M. Papadopoulou, P. Lafazani, M. Tsakiri - Strati,. (2009). Sun glint correction of very high spatial resolution images. *MDPI - Remote Sensing*, 697 - 730.
- John F. Mustard, Matthew I. Staid, William J. Fripp. (2001). A Semianalytical Approach to the Calibration of AVIRIS Data to Reflectance over Water: Application in a Temperate Estuary. *Elsevier- Remote Sensing of Environment*, 335 - 349.
- John Hedley, Alastair Harborne, Peter Mumby. (2005). Simple and robust removal of sun glint for mapping shallow-water benthos. *International Journal of Remote Sensing*, 2107 - 2112.
- Kerle, N. (2013). *Electromagnetic Radiation*. Verlag Berlin Heidelberg: Springer.
- Lee, Z., Carder, K. L., Mobley, C. D., Steward, R. G., & Patch, J. S. (1999). Hyperspectral remote sensing for shallow waters 2: Deriving bottom depths and water properties by optimization. *Applied Optics*, 38 (18), 3831-3843.
- Lyzenga, D. R. (1978). Passive remote sensing techniques for mapping water depth and bottom features. *Applied Optics*, 17, 379 - 383.
- Lyzenga, D. R. (1985). Shallow water bathymetry using combined lidar and passive multispectral scanner data. *International Journal of Remote Sensing*, 115-125.
- Martin, S. (2014). *Introduction to Ocean Remote Sensing*. Cambridge: United Kingdom, MPG Printgroup Limited .
- Miller, C. I. (2012). *Evaluation of Sunlint Correction algorithms for high-spatial resolution hyperspectral imagery*. Montrey, California: Naval Postgraduate School.
- Polcyn, F.C., and Rollin, R.A. (1969). *Remote Sensing Techniques for the Location and Measurement of Shallow Water Features*. University of Michigan: Willow Run Laboratories.
- Richard P. Stumpf, Kristine Holderied, Mark Sinclair. (2003). Determination of water depth with high-resolution satellite imagery over variable bottom types. *Limnology and Oceanography*, 547-556.
- Shachak Pe'eri, Christopher Parrish, Chukwuma Azuike, Lee Alexander Andrew Armstrong. (2014). Satellite Remote Sensing as a Reconnaissance Tool for Assessing Nautical Chart Adequacy and Completeness. *Marine Geodesy* 37/ 3, 293 - 314.
- Tiit Kutser, Ele Vahtmäe, Jaan Praks. (2009). A sun glint correction method for hyperspectral imagery containing areas with non-negligible water leaving NIR signal. *Elsevier - Remote Sensing of Environment*, 2267 - 2274.

Westley, K. (2021). Satellite-derived bathymetry for maritime archaeology: Testing its effectiveness at two ancient harbours in the Eastern Mediterranean. *Elsevier - Journal of Archeological Science: Reports*.